
**Travail de fin d'études et stage[BR]- Travail de fin d'études : Cooling
Performance of Macro-Encapsulated Phase Change Material (PCM) Panels:
Experimental Investigation and FEM Modelling[BR]- Stage d'insertion
professionnelle : DTU**

Auteur : Chaudoir, Basile

Promoteur(s) : Lemort, Vincent

Faculté : Faculté des Sciences appliquées

Diplôme : Master en ingénieur civil électromécanicien, à finalité spécialisée en énergétique

Année académique : 2022-2023

URI/URL : <http://hdl.handle.net/2268.2/17561>

Avertissement à l'attention des usagers :

Tous les documents placés en accès ouvert sur le site le site MatheO sont protégés par le droit d'auteur. Conformément aux principes énoncés par la "Budapest Open Access Initiative"(BOAI, 2002), l'utilisateur du site peut lire, télécharger, copier, transmettre, imprimer, chercher ou faire un lien vers le texte intégral de ces documents, les disséquer pour les indexer, s'en servir de données pour un logiciel, ou s'en servir à toute autre fin légale (ou prévue par la réglementation relative au droit d'auteur). Toute utilisation du document à des fins commerciales est strictement interdite.

Par ailleurs, l'utilisateur s'engage à respecter les droits moraux de l'auteur, principalement le droit à l'intégrité de l'oeuvre et le droit de paternité et ce dans toute utilisation que l'utilisateur entreprend. Ainsi, à titre d'exemple, lorsqu'il reproduira un document par extrait ou dans son intégralité, l'utilisateur citera de manière complète les sources telles que mentionnées ci-dessus. Toute utilisation non explicitement autorisée ci-avant (telle que par exemple, la modification du document ou son résumé) nécessite l'autorisation préalable et expresse des auteurs ou de leurs ayants droit.

Cooling Performance of Macro-Encapsulated Phase Change Material (PCM) Panels: Experimental Investigation and FEM Modelling

Author :
Basile CHAUDOIR
S180583

Promoter :
Vincent LEMORT

Supervisor in DTU :
Ongun BERK KAZANCI

FINAL THESIS FOR THE AWARD OF A MASTER'S DEGREE
"INGÉNIEUR CIVIL ÉLECTROMÉCANICIEN, À FINALITÉ SPÉCIALISÉE EN
ÉNERGÉTIQUE"

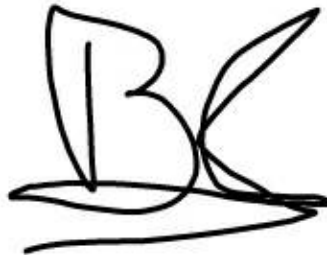
Academic Year 2022-2023

Preface

The thesis has been prepared over the course of an internship over five months. It accounts for 30 ECTS credits and is part of the following degree in Uliège : "Master : ingénieur civil électromécanicien, à finalité spécialisée en énergétique". The research took place at Technical University of Denmark DTU from the 9th of February to the 9th of June.

I express my gratitude to : Associate Professor Ongun B. KAZANCI, Post doc. Jun SHINODA, PhD Dragos-Ioan Bogatu, Professor Vincent LEMORT and PhD Alanis Zeoli for their guidance and feedback. I would also like to thank my friend Yanghao Cui for his help while conducting experiments.

9th of June 2022

A handwritten signature in black ink, consisting of a large, stylized letter 'B' with a vertical line through it, followed by a flourish that extends to the right and then loops back under the 'B'.

Abstract

This thesis aimed to investigate macro-encapsulated PCM panels (MEP) facing a high heat load. Another goal was to use Finite Element Method (FEM) to model MEPs and to analyse with precision more simple models as can be used in other simulation tools such as TRNSYS.

The experimental investigation showed that ventilation parameters (inlet temperature and flowrate) and water circulation parameters (temperature setpoints for activation) determined the MEPs behaviour. This behaviour could be similar to TABS (when ventilation was dominant in terms of cooling during occupancy) or to a radiant ceiling (when the cooling impact of ventilation was reduced). By choosing the values of these parameters well, it was possible for the operative temperature to stay 95.8% of the time in Category II (including 92.1% of the time in Category I) according to EN 16798-1. It also showed that day-active water circulation could improve panel heat absorption by 35% with deactivated ventilation (reaching 21 W/m^2 in average during occupancy).

Three models were designed using FEM. One day of panel behaviour was simulated for each of them. A realistic model was validated using a criteria involving RMSEs on panel surface temperature and heat flux using measurements from the experimental campaign. A second model was designed using a simpler structure that could be implemented in other softwares. It could be validated using temperature measurements and values of heat flux computed from a theoretical formula. A comparison of these models regarding vertical stratification of PCM temperature showed that fins in the panel aluminum profile supporting the cooling water pipes enhanced thermal conductivity of the PCM layer. A third model was designed by using the same geometry as the Type399 TABS model of TRNSYS and by altering some PCM properties (density and thermal conductivity). This model could also be validated using temperature measurements and heat flux values from the same theoretical formula as the second model.

Contents

1	Introduction	1
1.1	Context	1
1.2	Thesis Objectives and Structure	1
2	Introduction to Phase Change Materials (PCMs)	3
2.1	Description of PCM	3
2.2	Important Properties	4
2.2.1	Benefits	4
2.2.2	Disadvantages	4
2.2.3	Design Parameters	4
2.3	Types of PCM	5
2.4	Applications of PCM Technologies in Buildings	5
3	Experimental State-of-the-art	7
3.1	Indoor Environment Standards Related to Operative Temperatures	7
3.2	Indoor Environment Standards Related to Ventilation	8
3.3	Bibliographic Review	9
3.4	DTU's System Timeline	10
3.5	Purpose of the Experimental Investigation	10
4	Methods	11
4.1	Rubitherm RT24	11
4.2	PCM Integration Technology	12
4.3	Test Chamber	13
4.4	System Instrumentation	16
5	Experiments	19
5.1	Summary of Scenarios	19
5.2	Effect of Increased Heat Gains	20
5.2.1	Reference Scenario	20
5.2.2	Investigation on Cooling Demand	21
5.2.3	Increased Heat Gains	22
5.2.4	Results	24
5.3	Day-active Water Control and Set-points	26
5.4	Addition of Ventilation	29
5.5	Recovery Scenario	32
5.6	Attempt of Tight Control	33
5.7	Discussion	36

6	Introduction to Finite Element Method	38
6.1	Brief Description of the Method	38
6.2	Advantages of the Method	39
6.3	FEM-Linked Bibliographic Review	40
7	Presentation of the Model	41
7.1	Geometry and Materials Definition	41
7.2	Model Assumptions	43
7.3	Meshing and Choice of Element Size	44
7.4	Simulation Definition	46
8	Results and Model Validation	48
8.1	Non-Occupancy Simulation	48
8.2	Occupancy Simulation	49
8.3	Model Validation	50
8.4	Study on Water Heat Extraction	51
9	Alternative Model : Simpler Model	52
9.1	Definition of the Model	52
9.2	Model Simulation	53
9.3	Validation	54
9.4	Study on Water Heat Extraction	55
9.5	PCM Temperature Stratification Comparison	56
9.6	Discussion	58
10	Other Geometry : Model Derived From TABS	59
10.1	Geometry, Assumptions and Materials Definition	59
10.2	Choice of Meshing Size and Simulation	61
10.3	Results and Validation	61
11	Discussion	64
12	Conclusion	65
A	Solar Heat Gain Schedule (SHG1)	70
B	Lab Temperatures for All Scenarios	70
C	Models Technical Drawings	71

List of Figures

1	Solid-Liquid PCM Working Principle [5].	3
2	Classification of PCMs [13].	5
3	RT24 distribution of specific heat capacity with respect to temperature [29].	11
4	Simplified drawing of the MEP [30].	12
5	Cross-section of MEP with sensors [24].	12
6	Picture and representation of the roof with the water circulation circuit and sensor placement [32].	13
7	Picture of heat gain devices in chamber 6.	14
8	Displacement Ventilation [33].	15
9	Pictures of the displacement ventilation diffuser (left) and exhaust (right).	15
10	Mounting of a surface temperature sensor (left) and of a heat flux sensor (right).	16
11	Air temperature sensors on stand.	17
12	Chamber 6 disposition for the reference scenario (IHG1).	20
13	Internal and solar heat gains per panel area for the reference scenario (IHG1 and SHG1).	21
14	Energy stored in the PCM panels compared with the cooling demand with respect to the number of occupants.	22
15	Chamber 6 disposition for the reference scenario (IHG2).	22
16	Internal and solar heat gains for the 6OCC scenario (IHG2 and SHG1).	23
17	Operative temperature, water circulation flowrate and mean panel heat flux evolution of REF and 6OCC scenarios.	24
18	Total heat gains, heat extraction and losses through walls of REF and 6OCC scenarios (over a day).	25
19	Comparison of thermal comfort categories time shares of operative temperatures for REF and 6OCC.	26
20	Operative temperature, water circulation flowrate and mean panel heat flux evolution of 6OCC, 25SP and 23SP scenarios.	27
21	Total heat gains, heat extraction and losses through walls for 6OCC, 25SP and 23SP scenarios (over a day).	28
22	Comparison of thermal comfort categories time shares of operative temperatures for 6OCC, 25SP and 23SP scenarios.	28
23	Operative temperature, water circulation flowrate and heat removal per panel area evolution of 25SP and 25SPV scenarios (operative temperature is common to the two technologies for 25SPV).	30
24	Total heat gains, heat extraction and losses through walls for 25SP and 25SPV scenarios (over a day).	31
25	Comparison of thermal comfort categories time shares of operative temperatures for 25SP and 25SPV scenarios.	31
26	Operative temperature, water circulation flowrate and heat removal per panel area evolution of the 3PM scenario (operative temperature is common to the two technologies).	33

27	Operative temperature, water circulation flowrate and heat removal per panel area evolution of 25SPV and TIGHT scenarios (operative temperature is common to the two technologies for both scenarios).	34
28	Total heat gains, heat extraction and losses through walls for 25SPV and TIGHT scenarios (over a day).	35
29	Comparison of thermal comfort categories time shares of operative temperatures for 25SPV and TIGHT scenarios.	35
30	Comparison of thermal comfort categories time shares of operative temperatures for all scenarios.	36
31	Representation of the basic concepts of Finite Element Method [39].	38
32	Examples of FEM applications aiming to study polymers [40].	39
33	Picture of a pipe profile.	41
34	2D model of a fin with materials description.	41
35	Minimum element size area definition (in yellow).	44
36	Temperature distribution in the panel for a steady-state simulation (in °C).	45
37	CPU time with respect to minimum element size.	45
38	Panel center temperature with respect to minimum element size.	45
39	Non-occupancy simulation boundary conditions.	46
40	Occupancy simulation boundary conditions.	47
41	Model central panel surface data comparison with experimental data (non-occupancy).	49
42	Model central panel surface data comparison with experimental data (occupancy).	49
43	Heat extracted through the copper tube from the air layer and the aluminium fin.	51
44	Geometry, materials and stratification nomenclature of PCM sub-layers of the simpler model.	52
45	Simpler model comparison with experimental data and first model (non-occupancy).	53
46	Simpler model comparison with experimental data and first model (occupancy).	54
47	Heat extracted through the copper tube from the air layer and the aluminium fin (simple model).	55
48	Comparison of the PCM temperature stratifications of the 2 models (non-occupancy).	56
49	Comparison of the PCM temperature stratifications of the 2 models per layer (non-occupancy).	57
50	Comparison of the PCM temperature stratifications of the 2 models (occupancy).	58
51	Geometry of the TABS model as modelled in TRNSYS [48].	59
52	2D TABS equivalent model geometry with materials description.	60
53	2D TABS equivalent model mesh.	61
54	TABS equivalent model comparison with experimental data and simpler model (non-occupancy).	62
55	TABS equivalent model comparison with experimental data and simpler model (day).	63
56	Heat rate and schedule of the experimental solar heat gains (SHG1).	70

LIST OF FIGURES

57	Lab Temperatures for All Scenarios.	70
58	2D model technical drawing.	71
59	2D simpler model technical drawing.	71
60	2D TABS equivalent model technical drawing.	72

List of Tables

1	PPD and thermal sensation with respect to PMV [19].	7
2	Categories of thermal comfort for operative temperature [18].	8
3	Parameters of indoor air quality for different categories based on perceived air quality [18].	9
4	ΔC_{CO_2} for different categories of indoor air quality [18].	9
5	RT24 Properties [29]	11
6	Summary of relevant sensor characteristics	18
7	Experimental scenarios overview.	19
8	Internal heat gains for the reference scenario (IHG1)	20
9	Internal heat gains for the 6OCC scenario (IHG2)	23
10	Summary of relevant results regarding heat extraction for all scenarios (specific values are provided relative to panel surface area).	37
11	Mean panel heat fluxes for various conditions for all scenarios [W/m^2].	37
12	Materials used from the NX library for the model and their characteristics.	42
13	Materials used from the NX library for the model and their characteristics.	42
14	Indicators for validation of the model for the two simulated time periods.	50
15	Indicators for validation of the simpler model.	54
16	Indicators for validation of all 3 models.	63

1 Introduction

1.1 Context

In recent years, climate change and its consequences have been the center of attention of many organisms as the European union. The latter set several milestones regarding climate change. For example the 2030 Climate Target Plan had as key elements a reduction of at least 55% of green house gas emissions compared to 1990 levels, at least 32% share for renewable energy and 32.5% improvement in energy efficiency [1]. This will set a path for the next target of the EU which is to become climate-neutral by 2050 [2].

Energy use related to buildings has a significant importance with respect to these goals. Indeed, the International Energy Agency (IEA) states that buildings and buildings construction sectors account for 30% of total global final energy consumption and 27% of total energy sector emissions [3]. Still according to the IEA, nowadays air conditioners and electric fans for cooling accounts for about 20% of total electricity used in buildings around the world. Their number is still growing could reach more than 60% of world's household by 2050. This would lead the energy demand for space cooling to triple by that time [4].

Numerous studies have been conducted in order to lower the environmental impact of cooling in buildings without compromising on thermal comfort. Most consisted in either improving existing technologies or introducing new ones. A part of these technologies rely on the inclusion of Phase Change Materials (PCM). Due to their high energy density, they allow to improve thermal mass of buildings by using a limited amount of space compared to sensible heat storage. As other heat storage, they allow shift the cooling load [7] which has many benefits such as reducing the strain put on electrical networks during peak hours. Other benefits are an improvement of energy efficiency [8] and of thermal comfort by reduction of temperature fluctuations inside a building. [9].

However, the literature lacks of research on PCM applications in buildings facing a high heat load. Also, most simulation softwares do not allow precise modelling of technologies such as macro-encapsulated PCM panels (MEP).

1.2 Thesis Objectives and Structure

This thesis first aimed to perform an experimental investigation of the behaviour of macro-encapsulated PCM panels when facing a high cooling load. The effect of day-active water circulation was also monitored in that regard to determine whether these panels can be used as conventional radiant panels.

This experimental part translates in:

- an introduction to PCMs (characteristics, classification and applications),
- a state-of-the-art relating to PCM uses in building as well as a presentation of standards related to indoor air quality and thermal comfort,
- a presentation of the experimental setup,
- the presentation of a set of experimental scenarios and their related results.

Secondly, a simulation oriented investigation used Finite Element Method (FEM). Three models were created to verify how changes on geometry based on assumptions would impact the model precision.

This simulation oriented part translates in:

- an introduction to Finite Element Method containing a short bibliographic review of uses of this tool related to radiant systems and PCMs.
- the design and validation of a realistic model based on a real pipe profile. A short study on heat absorption during water circulation was also conducted.
- the design and validation process of a model having a simpler geometry. A comparison on PCM temperature stratification was performed to assess the impact of the panel structure on the contained PCM.
- the design and validation process of a model having a geometry similar to the TRNSYS Type399 model for Thermally Activated Building System (TABS).

2 Introduction to Phase Change Materials (PCMs)

This section aims to provide a succinct description of PCM and their technologies. It presents:

- the working principle of PCMs,
- their critical properties,
- a list of the different types of PCM,
- possible applications of this technology in buildings.

This section mainly focuses on the relevant information related to the topics of this thesis.

2.1 Description of PCM

As their name suggests, phase change materials are substances designed to absorb and release heat during their transition between two phases (e.g. solid and liquid). They are often used as heat storage. In building applications, the chosen phase change is usually the liquid-solid one (in the targeted temperature range). This is due to the smaller density change these states have between each other compared to the liquid-gas phase change.

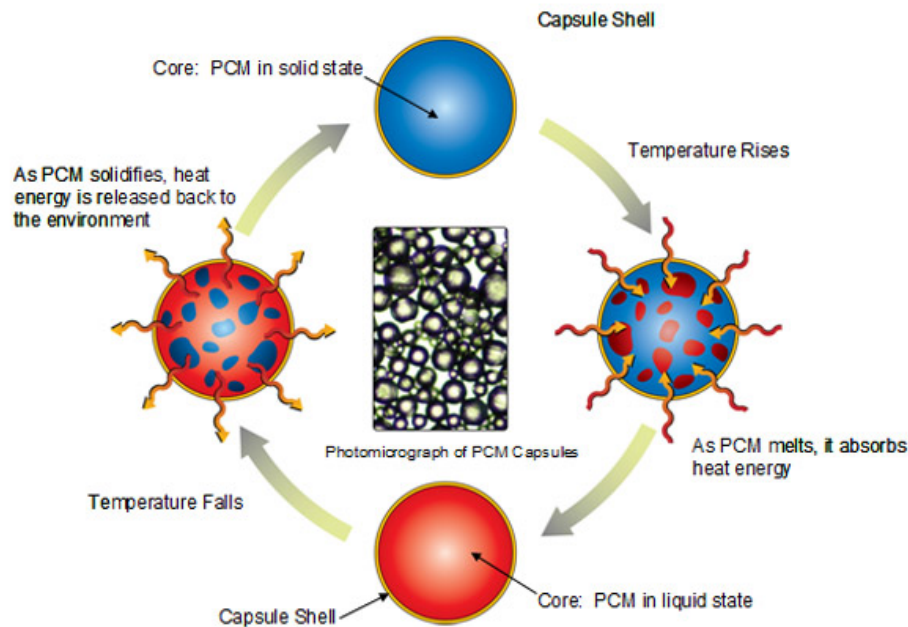


Figure 1: Solid-Liquid PCM Working Principle [5].

As shown in Figure 1, the liquid PCM releases latent heat when in a colder environment which causes its solidification. Then when the ambient temperature increases, the heat is absorbed by the solid PCM which melts in consequence. This cycle can help to damp temperature oscillations when these are around the phase change range of the PCM.

2.2 Important Properties

2.2.1 Benefits

The main benefit of Phase Change Materials is that they have a high thermal heat density over a possibly small temperature range. Their latent heat can range from 120 to 250 kJ/kg (for pure materials) depending on the type of PCM [6]. In comparison, a sensible heat storage mainly composed of water would have a heat capacity of about $4.2 kJ/(kg \times K)$. This means that over their phase change range, PCM can have a much higher energy density and be used as very effective thermal energy storage (TES). The latter technology has many benefits:

- peak-shaving and load shifting, allowing to also benefit from an off-peak energy tariff [7],
- increase of energy efficiency as coupling radiant heating/cooling systems with PCM allows to reduce the loads (and thus the grid electricity consumption) in some cases [8],
- reduction of temperature fluctuations leading to better thermal comfort if the phase change temperature range of the PCM overlaps the operative temperature range of the building [9].

Another benefit is that those materials can be applied in a large range of different technologies. These all also have their own benefits and disadvantages. Some of these will be discussed in Section 2.4.

2.2.2 Disadvantages

However, PCM suffer from several drawbacks, one of the most popular as research topic research being the low heat conductivity of these materials. This low value causes non uniform temperature profiles in the PCM, hence leading to an heterogeneous phase change of the material and a lower heat absorption/release rate. Lots of studies try to enhance this property by either considering the effect of non-moving structures (i.e. structures inserted inside the PCM layer to serve as a heat conductivity bypass) [10] or nano-particles (i.e. molecules mixed with the PCM to act on its properties) [11].

Another problem of PCM technologies is their high production costs. Nonetheless, some technologies can still have a competitive operational cost that can in some situations (high cooling demand) compensate for this high initial cost compared to conventional systems [12]. Furthermore, other inconveniences related to the type of PCM can be enumerated and will be discussed in Section 2.3.

2.2.3 Design Parameters

Apart from benefits and drawbacks, PCM have some design parameters that can be adjusted. The main one is the phase change temperature range. This range determines the temperature range where the thermal inertia will be added. When integrated inside a building, matching the material phase change temperature range with the building operative temperature range is required for the technology to be effective [9].

2.3 Types of PCM

From what can be seen in the literature, phase change materials can be divided into three main categories with respect to the type of materials [13]. A representation of these categories and their main sub-categories can be found in Figure 2.

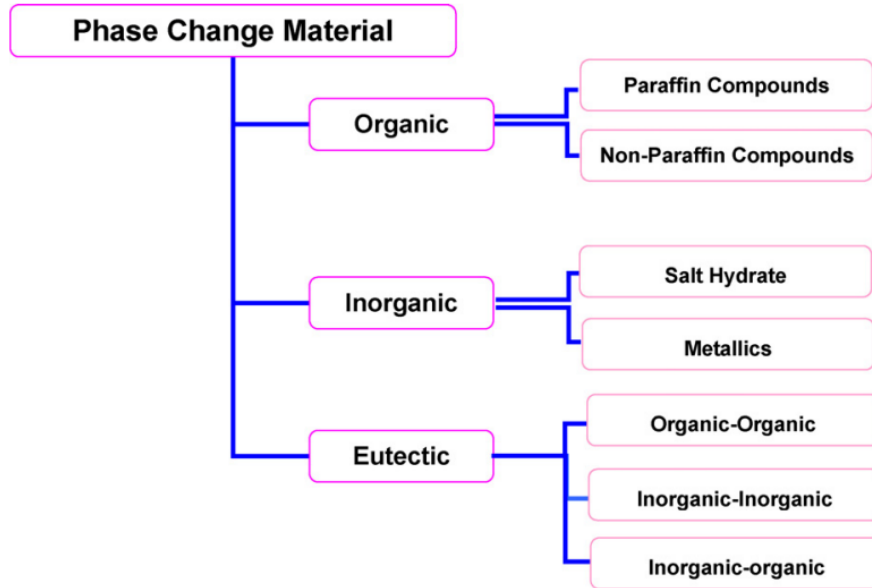


Figure 2: Classification of PCMs [13].

- **Organic compounds** : This category includes paraffin compounds, esters, acids, alcohols & glycol substances. Phase change materials of this type have a more stable performance. On the other hand, they have a low thermal conductivity and can have flammability issues.
- **Inorganic compounds** : This category regroups mainly salt hydrates & metals. These usually have better performances as their energy density and thermal conductivity are higher. However, they can corrode their containers (made of metallic and gypsum materials).
- **Eutectic compounds** : These compounds are a mix of the 2 latter categories. The goal is to minimize flaws while taking advantage of each categories' benefits.

2.4 Applications of PCM Technologies in Buildings

As previously stated, phase change materials can be used in buildings in order to increase their thermal inertia. There are many ways to introduce them in a building. The main ones are:

- **Impregnation** : Which consists in submerging a porous matrix into PCM in order to enhance that matrix with a higher thermal mass. This technology's main problem is the leakage of the material [14].
- **Shape stabilization** : This consists in containing PCM in a matrix and by making sure that its shape doesn't change when the materials fuses or solidifies. This technology prevents leakage but reduces thermal conductivity of the structure while increasing the costs [15].

- Micro-encapsulation of PCM : This method can be realized by pouring a mix of gypsum and PCM (in the form of a powder) in structures (e.g. a panel). This eliminates leakage and flammability issues. However, this leads to a decrease in the overall thermal conductivity of the structure and an increase in costs [16] [17].
- Macro-encapsulation of PCM : This method consists in filling a container (e.g. a tube, a box) with pure PCM. This method has a great energy density and is simple to put into place. However, the main inconveniences are flammability, potential leakages and a potential non-uniform solidification of the material leading to lower performances [17].

3 Experimental State-of-the-art

This section aims to present the used standards related to indoor environment and past work on PCM integration in buildings. The past work description was subdivided in the following parts:

- The first section, containing broad examples of studies on PCM in buildings will be provided. These examples could contain different or similar experimental setups compared to the one used for this study.
- The second section, focusing on studies made in DTU. The setup is using macro-encapsulated panels. This sub-part will aim to describe how the setup used for this thesis behaved in past experiments and what are its main parameters (these will be detailed more completely in Section 4).
- Finally, a section discusses the observations from the literature. This discussion leads to the decisions of the experiments made during this thesis.

3.1 Indoor Environment Standards Related to Operative Temperatures

The standard used in this study are described in the EN 16798-1:2019 document [18]. The standard describes ranges for thermal comfort called Categories, which are based on the PPD-PMV method (Predicted Percentage of Dissatisfied - Predicted Mean Vote).

PPD-PMV is a systematic method detailed in ISO 7730 [19]. It expresses the value of the Predicted Mean Vote (being between -3 and 3) in terms of several variables (metabolic rate, clothing, relative humidity, average radiation temperature, air flowrate and indoor temperature). The PMV value is associated with a thermal comfort feeling as represented in Table 1:

Table 1: PPD and thermal sensation with respect to PMV [19].

PMV	-3	-2	-1	-0.5	0	-0.5	1	2	3
PPD [%]	100	75	25	10	5	10	25	75	100
Thermal sensation	Cold	Cool	Slightly cool		Neutral		Slightly warm	Warm	Hot

From this PMV value, it is possible to compute the PPD (Predicted Percentage of Dissatisfied) value as in Equation 1 [19]:

$$\text{PPD} = 100 - 95e^{-(0.03353\text{PMV}^4 + 0.2179\text{PMV}^2)} \quad (1)$$

This equation takes into consideration the fact that not everyone has the same perception of thermal comfort. Some values of PPD are represented in Table 1 with respect to PMV.

From this method, categories can be created regarding thermal comfort (see Table 2). These categories have been used as performance indices in the experimental investigation.

Table 2: Categories of thermal comfort for operative temperature [18].

Category	I	II	III	IV
PPD [%]	< 6	< 10	< 15	< 25
$RANGE_{T,c}$ [$^{\circ}C$]	23.5-25.5	23-26	22-27	21-28

$RANGE_{T,c}$ is the range of operative temperature for a cooling season with occupants having a clothing of 0.5 clo (summer clothing). The goal in office buildings is to have the operative temperature staying as much as possible in Category II of thermal comfort. Category I is aimed at in buildings having occupants sensible to effects of temperature (e.g. retirement homes, hospitals).

3.2 Indoor Environment Standards Related to Ventilation

A similar approach as in last section using expected percentage of dissatisfied (EPD) can be also used for ventilation flowrates during occupancy. This allows to associate design ventilation flowrates to air quality categories depending mainly on the size of the room and the number of occupants. Two methods detailed in the DS/EN 16798-1:2019 document [18] will be used. The first method is based on perceived air quality and the second one uses limit values of substance concentration. The ventilation flowrates in the experiments were set to fit in Category II. Note that apart from the categories, a minimum of 4 L/s is required per occupant in buildings.

Method Based on Perceived Air Quality

This method uses coefficients to compute the design flowrate as in Equation 2:

$$q_{des} = n_{occ} \times q_{occ} + A_{floor} \times q_{floor} \quad (2)$$

- q_{des} is the design flowrate for the room [L/s].
- n_{occ} is the number of occupants in the room.
- q_{occ} is the flowrate required per occupant (this depends on the desired indoor air quality) [$L/(s \times pers)$]. In this study, these coefficients will be considered for non-adapted person.
- A_{floor} is the floor area of the room [m^2].
- q_{floor} is the flowrate required per unit of building area (this depends on the desired indoor air quality) [$L/(s \times m^2)$]. In this study, these coefficients will be considered for low polluting buildings.

The values for the parameters q_{occ} and q_{floor} can be found in Table 3:

Table 3: Parameters of indoor air quality for different categories based on perceived air quality [18].

Category	I	II	III	IV
EPD [%]	15	20	30	40
q_{occ} [$L/(s \times pers)$]	10	7	4	2.5
q_{floor} [$L/(s \times m^2)$]	1	0.7	0.4	0.3

Method using Limit Values of Substance Concentration

This method uses design values of CO_2 concentrations above outdoor concentration if a person emits a standard value of 20 [L/h] of CO_2 (named ΔC_{CO_2}). These values are listed in Table 4. Finally, the design flowrate can be computed as in Equation 3.

Table 4: ΔC_{CO_2} for different categories of indoor air quality [18].

Category	I	II	III	IV
EPD [%]	15	20	30	40
ΔC_{CO_2} [PPM]	550	800	1350	1350

$$q_{des} = \frac{CO_{2gen} \times n \times 10^6}{\Delta C_{CO_2} \times \eta_v} \quad (3)$$

- q_{des} is the design flowrate for the room [L/s].
- n_{occ} is the number of occupants in the room.
- CO_{2gen} is the generated CO_2 volume per occupant [$l/(s \times pers)$]. Here, from previous assumption for the coefficients, this is equal to $\frac{20}{3600} = 0.0056$ [$l/(s \times pers)$].
- η_v is the ventilation efficiency that will be assumed to 1.

When the room is not occupied, the ventilation is turned off except during the two hours prior to occupancy. As the standard [18] suggests, there are two ways to ventilate the room properly outside of occupancy to ensure fresh air for the occupants at their arrival:

- perform one air change within two hours prior to occupancy.
- ventilate 0.15 $l/(s \times m^2)$ outside occupancy.

3.3 Bibliographic Review

Weinläder et. al. [20] compared two designs of a PCM radiant panel composed of two main layers (i.e. one of graphite and one of PCM) and a water circulation structure. The comparison was made on a performance criteria and the difference between these designs was the vertical position of the layers. The researchers concluded that having the PCM below the graphite layer and the circulating water resulted in a better thermal connection between the PCM and the room.

Gallardo et. al. [21] simulated the performance of a radiant panel system with integrated PCM in very hot and humid conditions. They showed that the system could save around 48% of operation energy compared to an all-air system in existing office buildings. These savings were mainly due to the operation of the cold generating plant at night.

Mousavi et. al. [22] designed and studied the performance of an experimental system composed of shape-stabilised PCM composite boards. They concluded that the system required 4-5h of water circulation during the night and that the panel system had a heat transfer coefficient of $8.48 \pm 0.97 \text{ W}/(\text{m}^2 \times \text{K})$.

3.4 DTU's System Timeline

Several experiments have been done to investigate the performance, efficiency and cost-efficiency of a PCM ceiling panel with embedded pipes for water circulation. Allerhand et. al. [23] aimed to compare macro-encapsulated panel prototypes with all-air systems and with TABS and showed that it had potential in becoming a new HVAC technology usable for building retrofitting.

Several studies focused on performance. Many parameters were varied (this list will mainly focus on studies done with the same experimental setup in DTU as the one used in this thesis):

- The water flowrate [24] which proved not to make a significant gap in performance. On the other hand, the circulating water temperature showed to have a much more significant impact [25].
- The ventilation type that is used with the technology. The latter is required to satisfy air quality standards. Results showed that displacement ventilation performed better than mixing ventilation in that regard [26].
- The heat load. Indeed, the value of heat gains (e.g. the number of people in the room was increased from 2 to 4) had a big impact on performances (more than 60 % of increase in average panel heat flux when ventilation is not activated)[27].
- Other ventilation parameters were also varied (air inlet temperature and flowrate) and showed drastic differences in performance (increasing the inlet air temperature or reducing the flowrate proved to lower significantly the performances of the system) [27].

Finally, the operational cost of the technology was also studied by Boccardo et. al. [28] and was compared to TABS (Thermally Activated Building Systems) and an all-air system. It showed that the PCM panel system had a high initial cost but a lower operating cost. In the end, the profitability compared to an all-air system depended on the cooling load (the latter were more profitable for small loads). However, TABS were always cheaper in that study.

3.5 Purpose of the Experimental Investigation

Previous sections described several investigations concerning various PCM technologies in buildings with a focus on macro-encapsulated PCM panels. However, some important scenarios remained to be studied. The system was for example never tested in extreme conditions (e.g. high cooling load).

The goal of this experimental part was to assess the maximal performance of the setup in an extreme configuration. To put it simply, parameters were varied in the context of an overcrowded room (with 6 people and 6 computers). More information about the scenarios is given in Section 5. This situation could correspond to a meeting or a project room. These experiments could also give insights of the ability of the system to recover the heat if it were stopped for maintenance or due to a system failure (e.g. black-out).

4 Methods

This section aims to provide a complete description of the experimental system : chamber 6 in the International Center of Indoor Environment and Energy (ICIEE) in DTU. In the end, this section contains :

- The characteristics of the phase change material (Rubitherm 24).
- The integration of this material in the panel.
- The test chamber layout.
- Details about the relevant sensors.

4.1 Rubitherm RT24

In this study, the phase change material used is the *Rubitherm RT24*. It is a pure organic PCM having a high heat capacity. In addition, it is chemically inert while having a stable performance. These assets ensure a long lifetime of this material. The properties of this material are summarised in Table 5 and in Figure 3 :

Table 5: RT24 Properties [29]

Phase Change Range	Total Heat Capacity	Specific Heat Capacity	Density Solid	Density Liquid	Heat Conductivity
21-25°C	160 kJ/kg	$2 \frac{kJ}{kg \times K}$	880 kg/m ³	770 kg/m ³	$0.2 \frac{W}{m \times K}$

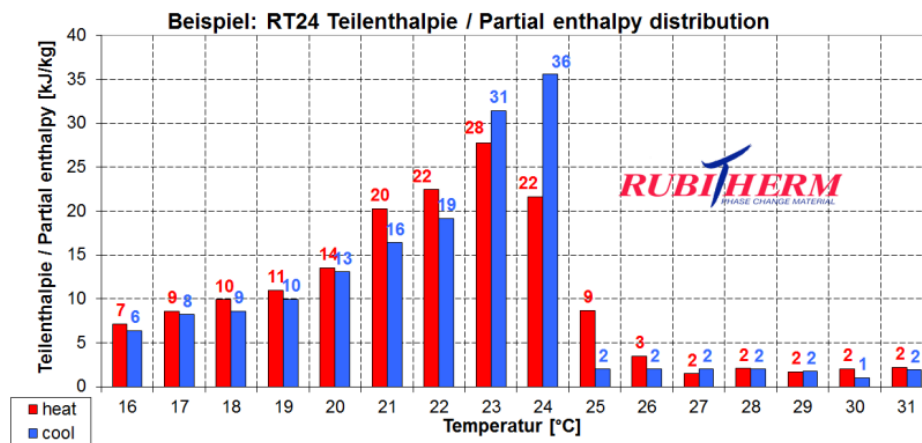


Figure 3: RT24 distribution of specific heat capacity with respect to temperature [29].

4.2 PCM Integration Technology

The technology used for this study is a **macro-encapsulated** PCM panel (MEP) containing pure Rubitherm RT24. This panel was designed in DTU and consists in a steel case with aluminium fins supporting copper pipes that circulate water. The fins and the pipes are partly submerged in PCM while the rest is filled with air. The fins aim to tackle the low thermal conductivity of the PCM and allow the heat to move more homogeneously from and to the PCM. The air is used as a thermal insulation between the PCM and the upper part of the panel. A simplified representation of this panel structure is shown hereafter (see Figure 4).

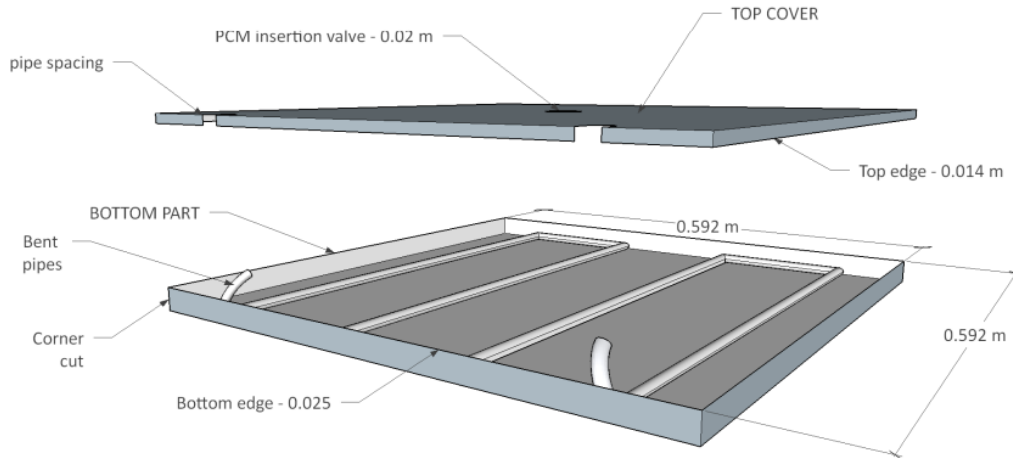


Figure 4: Simplified drawing of the MEP [30].

These panels are filled with approximately 3 kg of PCM. A representation of the cross section of a panel with sensor position is shown in Figure 5. More details about sensors will be given in Section 4.4.

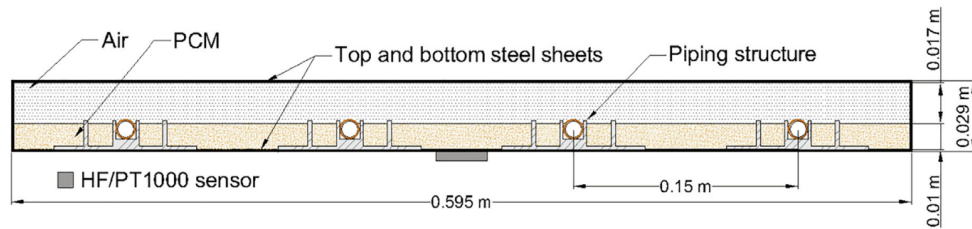


Figure 5: Cross-section of MEP with sensors [24].

4.3 Test Chamber

This section presents the chamber, the radiant ceiling, the water circulation system, the heat gains devices and the ventilation system. More information on the disposition of these elements will be given in Section 5.

Chamber General Information

This part describes the chamber as in the previous work from Bogatu et. al. [24] that used the same experimental setup. Chamber 6 aims to represent an office room. Its dimensions are 4.2 x 5.4 x 3.2 m (W x L x H). The chamber consists in three sections, the room representing the office space (2.7 m high), the plenum (0.5 m high) located above the room separated by a metal frame and the slab (under the room). The walls have a sandwich structure of mineral wool framed by two steel sheets and their heat transmission coefficient is of $0.25 \text{ W}/(\text{m}^2 \times \text{K})$ [31].

Chamber Ceiling and Water Circulation System

48 panels as presented in previous section are placed on the suspended frame of the test chamber. A panel surface is of about 0.36 m^2 , such that the total ceiling surface (A_{ceil}) accounts for around 17 m^2 . A schematic and a picture are shown in Figure 6.

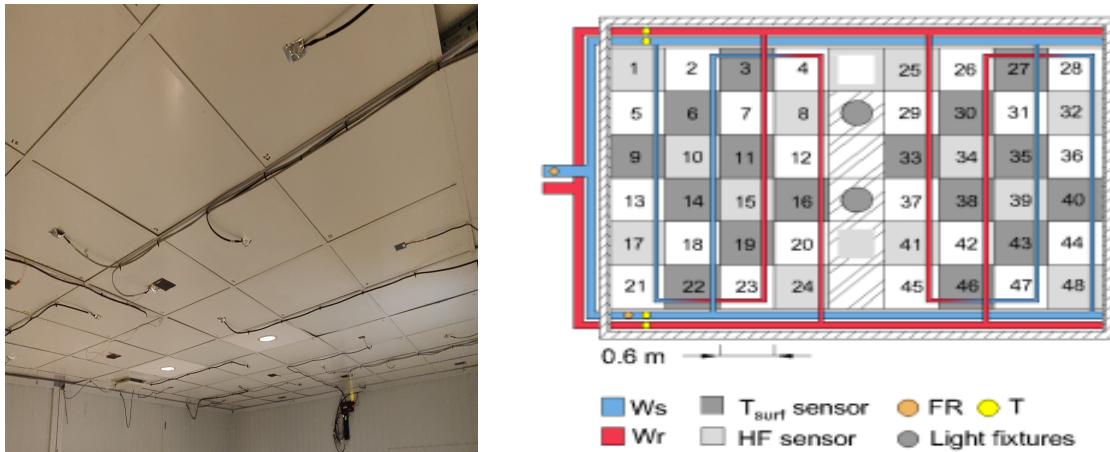


Figure 6: Picture and representation of the roof with the water circulation circuit and sensor placement [32].

The water circulation circuit is divided in two main supply and return loops. Each loop supplies and extracts water in two different locations. In the end, the system consists of four intake and exhaust of water. This is done in order to ensure an even distribution in terms of water temperature and flowrate. This circuit is implemented in practice with flexible connections between the panels.

Heat Gain Sources

There are four controlled heat gain sources in this test chamber. These are:

- a couple of lamps (see Figure 6),
- an electrical heating net that aims to emulate solar heat gains through a window,
- metal dummies equipped with a heat source (a light-bulb) to emulate human occupants and their heat generation,
- computers or radiant boxes equipped with light-bulbs that aim to emulate equipment heat gains.

The last three are shown in Figure 7.



Figure 7: Picture of heat gain devices in chamber 6.

Ventilation System

A displacement ventilation system is used in this study. This means that air will be supplied at floor level from a diffuser. This air will displace the warm and contaminated air above it to the ceiling where an exhaust is placed. The goal is to have a uniform air movement from a low non-inhabited location in the room going through the inhabited zone up to the ceiling (see Figure 8).

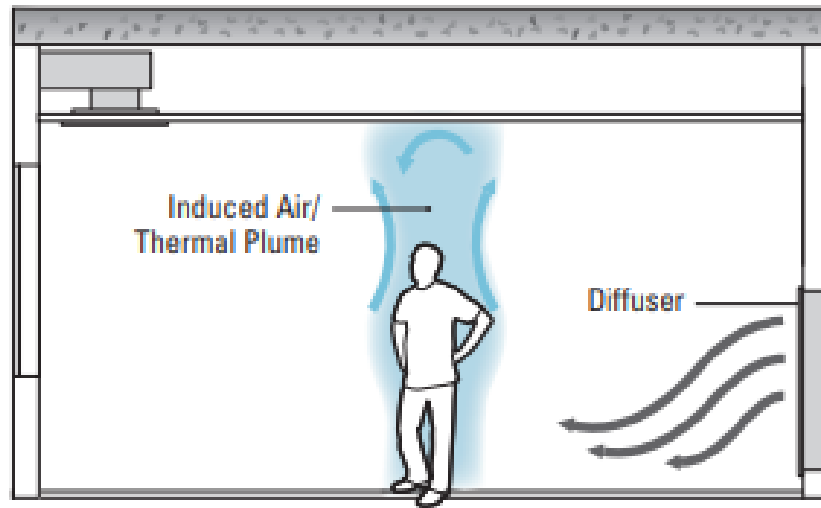


Figure 8: Displacement Ventilation [33].

The displacement ventilation diffuser used in chamber 6 is the CQA 1207 from Lindab. The exhaust is the LKA 125 from Lindab. Pictures of these devices are shown in Figure 9.



Figure 9: Pictures of the displacement ventilation diffuser (left) and exhaust (right).

4.4 System Instrumentation

Several sensors were used to monitor the test room conditions. Some mainly enable to know the behaviour of different panels located at different places in the ceiling (measuring their surface temperature and heat flux). Others are focused on water and air systems in order to compute energy balances on the system (they measure supply/exhaust temperatures and flow-rate). Finally, some aim to estimate heat losses through the walls (measuring wall surface temperatures and heat fluxes). A summary table of relevant sensor characteristics is shown at the end of this section (Table 6).

Surface Temperature Sensors

22 PT1000 temperature sensors are used to measure (in parentheses, the number of sensors used for this purpose):

- panel surface temperatures (16).
- chamber internal wall temperatures (4).
- the temperature on the heating net (1).
- a chamber external wall temperature (1).

Thermal paste was applied between the surface and the sensor in order to increase contact. A sponge was added on top of the sensor to insulate it from the room and the whole got covered with reflective tape to limit the effect of radiations on the measurement. Figure 10 shows the set of such a sensor:

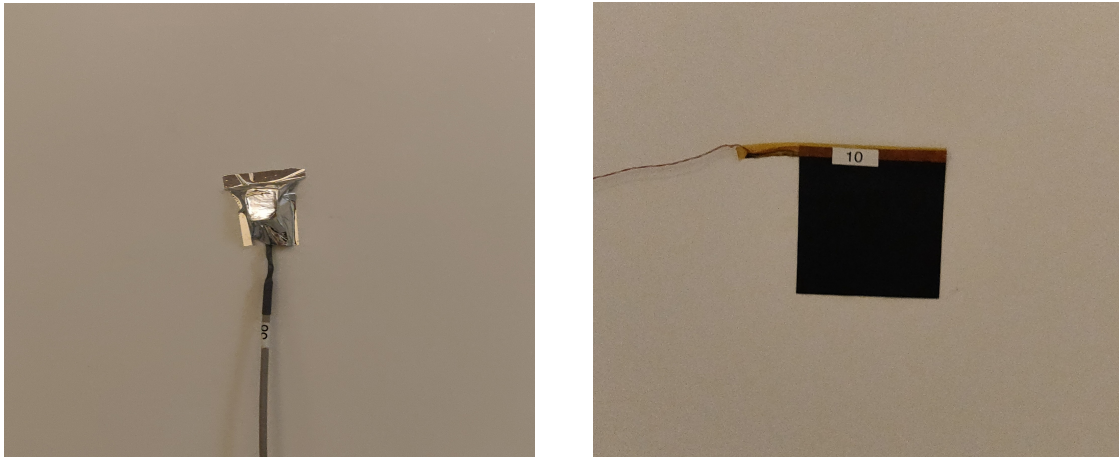


Figure 10: Mounting of a surface temperature sensor (left) and of a heat flux sensor (right).

Heat Flux Sensors

These sensors from gSKIN measure the heat flux between the room and the panel surface. This heat flux is composed mainly of convection and radiation. They will be necessary to assess the cooling power of the panels. They are mounted as in Figure 10.

Air Temperature Sensors

These PT1000 sensors are mounted on a stand as in Figure 11 (note that there are two stands in the chamber, more details on the disposition in the chamber in Section 5). They are used to measure the air temperature at four heights [0.1, 0.6, 1.1, 1.7] *m*. These heights were selected based on ISO 7726 [34]. They correspond respectively to the heights of ankle, abdomen and neck of a seated person and the height of the neck of a standing person. The sensor situated at height 0.6 m was used to measure the operative temperature of the room (abdomen level of a seated person). A globe sensor was used for this measurement as the operative temperature computation requires the air and the mean radiant temperatures [34].

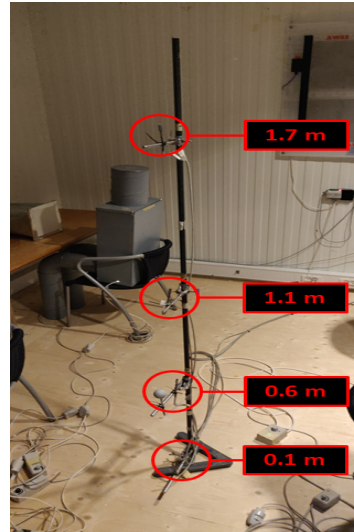


Figure 11: Air temperature sensors on stand.

Water Related Sensors

Two Kamstrup multical 602 sensor sets are used for the measurement of the flow rate and temperature of the circulating water for both of the circuit main divisions as can be seen in Figure 6 (the 2 top tubes and the 2 bottom tubes are the said main divisions and their temperatures and flowrate will be measured). These measurements will allow the chamber user to know how much energy has been extracted from the panels by the water when it is circulating.

Ventilation Related Sensors

Senso Anemo Series 5100NSF transducers are used for the ventilation supply and exhaust. They consist in an anemometer (measuring wind speed) and a temperature sensor. From the air speed and the ventilation tube section, it is possible to approximate the air flowrate with a fluid mechanics study. This can be used to compute the internal energy gain/removal in the chamber caused by the ventilation.

Sensor Calibration

All PT1000 sensors were calibrated prior to the experiments. For the rest of the sensors, the factory calibration sheet was used.

Sensor Summary

Table 6 displays the main information about the different sensors themselves. It also contains the links to sensor datasheets when available on the web. Panel sensors are disposed across the ceiling as in Figure 6.

Table 6: Summary of relevant sensor characteristics

Measured Variable	Sensor Name	Range	Accuracy/Rel. error
Temperature	PT1000 [35]	[-50 ; 500] °C	± 0.2%
Water Temperature	Kamstrup multical 602 [36]	[2 ; 180] °C	± 0.4%
Water Flowrate	Kamstrup multical 602 [36]	[0 ; 0.6] $\frac{m^3}{h}$	± 0.14 %
Heat Flux	gSKIN-XI 27 9C [37]	[-150 ; 150] $\frac{kW}{m^2}$	± 3 %
Air Temperature	SensoAnemo 5100NSF [38]	[-10 ; 50] °C	± 0.2°C
Air speed	SensoAnemo 5100NSF [38]	[0.05 ; 5] $\frac{m}{s}$	± 0.02 $\frac{m}{s}$ ± 1.5%

5 Experiments

This section presents all the experimental scenarios that were part of the study and compare results of similar ones. All of them were carried out with the experimental setup presented in the previous section during at least 4 days to ensure steady periodic-state (only the last day was used for the analyses). All scenarios consisted in two main phases:

- Occupation time (from 8:00 to 18:00). During this time interval, internal and solar heat gains are activated. In some scenarios, water can be actively circulated during the day if the operative temperature were to reach a previously defined day setpoint (Day SP). The system will then circulate water until the temperature reaches a temperature that is 1°C below that setpoint in order to limit the frequency of starts and stops of the water circulation pumps. This control strategy also limits overcooling.
- Non-occupation time (from 18:00 to 8:00). Internal heat gains are deactivated during this phase. The water circulation will also start until the room operative temperature reaches a temperature that is 1°C beneath a night setpoint (Night SP).

The ventilation has not been active for all scenarios. The solar heat gains are generated by the heating net (presented in Section 4.3) and simulate the solar heat gains from a south facing window (SHG1, the solar heat gain schedule can be found in Appendix A). The amount of solar heat gain and the related schedule were the same for all experiments. Finally, the same water circulation flowrate (\dot{m}_w) and temperature ($T_{w,s}$) were used for all scenarios (respectively 220 kg/h and 18 °C).

5.1 Summary of Scenarios

Table 7 summarises the different experimental scenarios. In bold are for each scenario the most important (or the only) change in parameters compared to previous ones. All elements in this table are detailed in next sections. IGH refers to the internal heat gains disposition and CTRL refers to the control strategy of water circulation, each of them is detailed in the presentation of their corresponding scenario. $T_{a,s}$ and \dot{m}_a are respectively the ventilation temperature and flowrate.

Table 7: Experimental scenarios overview.

Scenario [-]	\dot{m}_w [kg/h]	$T_{w,s}$ [°C]	IGH [-]	SHG [-]	$T_{a,s}$ [°C]	\dot{m}_a [m3/h]	CTRL [-]	Day SP [°C]	Night SP [°C]
REF	220	18	IHG 1	SHG 1	N/A	N/A	CTRL 1	N/A	22
6OCC	220	18	IHG 2	SHG 1	N/A	N/A	CTRL 1	N/A	22
25SP	220	18	IHG 2	SHG 1	N/A	N/A	CTRL 2	25	22
23SP	220	18	IHG 2	SHG 1	N/A	N/A	CTRL 2	23	22
25SPV	220	18	IHG 2	SHG 1	20	210	CTRL 2	25	22
3PM	220	18	IHG 2	SHG 1	20	210	CTRL 3	23	24
TIGHT	220	18	IHG 2	SHG 1	22	152	CTRL 2	23	23

In Appendix B are represented the different lab temperatures for all scenarios. Figure 57 shows that some scenarios had lab temperature that were different from the average scenario (e.g. the difference

can rise up to 2.5°C between TIGHT and REF). This can be due to lab occupancy or to the weather during the scenario. However, the difference in lab temperature for scenarios that were specifically compared in the following sections never topped 1.3°C . These differences in lab temperature could have an impact on wall heat losses and thus alter the accuracy of results.

5.2 Effect of Increased Heat Gains

This section provides a comparison between the reference scenario (REF) and a similar scenario with increased heat gains (6OCC). First, these two scenarios have to be detailed.

5.2.1 Reference Scenario

The REF scenario has been conducted to verify the proper operation and measurement of the system. It also serves as a baseline for comparison with other scenarios. The configuration inside the chamber is represented in Figure 12.

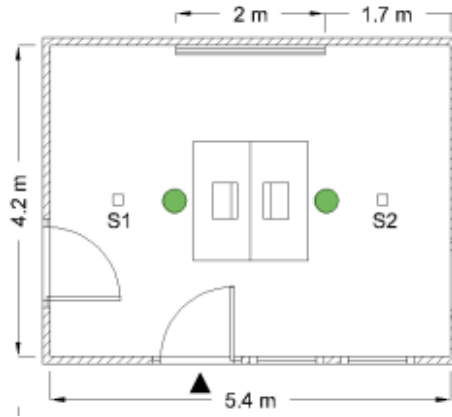


Figure 12: Chamber 6 disposition for the reference scenario (IHG1).

The configuration consists in the use of the chamber by two dummies (in green) mimicking the heat gains of two sitting people using two computers. The two stands (presented in Section 4.4) for the room temperature measurements are placed in the S1 and S2 spots. Other heat gains are the two lights that can be seen in Figure 6. Table 8 lists the different sources of heat gains (to the same values as in the study of Bogatu et. al. [24]).

Table 8: Internal heat gains for the reference scenario (IHG1)

Device [-]	Number [-]	Unit heat rate input [W]	Total heat rate input [W]
Lights	2	18	36
Dummies	2	75	150
Computers	2	50	100
TOTAL	/	/	286

Internal and solar heat gains constitute most of the heat input in the chamber. They have been plotted per panel area with respect to time for a day in Figure 13. Most results related to performance were divided by the total panel area in order to have results non-dependent on the size of the experimental setup. As a reminder, the total area covered by the panels is of about 17 m^2 .

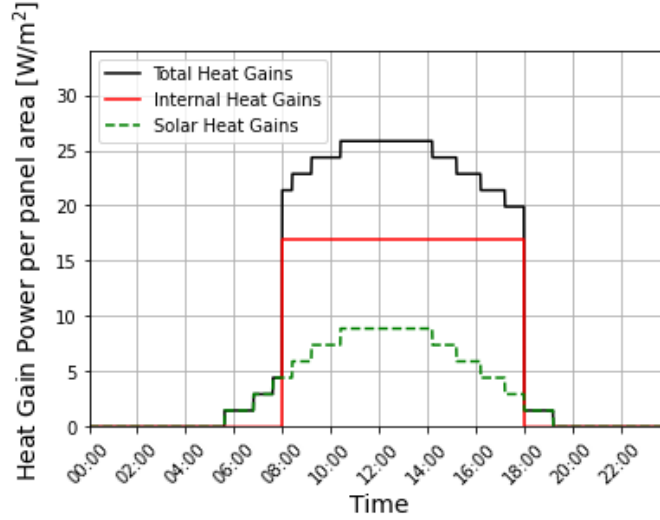


Figure 13: Internal and solar heat gains per panel area for the reference scenario (IHG1 and SHG1).

Concerning the water circulation, it has been deactivated during the day, allowing the panels to absorb heat passively from the room. From 18:00, the water circulation was activated if the operative temperature exceeded the night setpoint. It would be active until the operative temperature in the room reached 21°C (as the setpoint is 22°C). This strategy has been referred to as CTRL 1. The ventilation has been deactivated.

5.2.2 Investigation on Cooling Demand

A fast investigation has been conducted to determine a rough estimation of the number of occupants that would generate more energy than what the PCM in the system could contain. The number of occupants was thus varied and their internal heat gains summed with the solar heat gains were integrated on a one day period. The melting energy required for all PCM panels ($E_{PCM,m}$) and the energy required to heat them from 20 to 26°C ($E_{PCM,20-26}$) were also computed as follows:

$$E_{PCM,m} = m_{PCM} \times n_{panels} \times h_m$$

$$E_{PCM,20-26} = m_{PCM} \times n_{panels} \times h_{20-26}$$

- m_{PCM} is the mass of PCM in a panel (approximated to 3.06 kg for all panels).
- n_{panels} is the number of panels in the ceiling (= 48).
- h_m and h_{20-26} are respectively the melting specific energy (from 21 to 25°C) and the specific energy to heat the PCM from 20 to 26°C . These can be determined using the data in Section 4.1.

The results of these computations have been plotted in Figure 14.

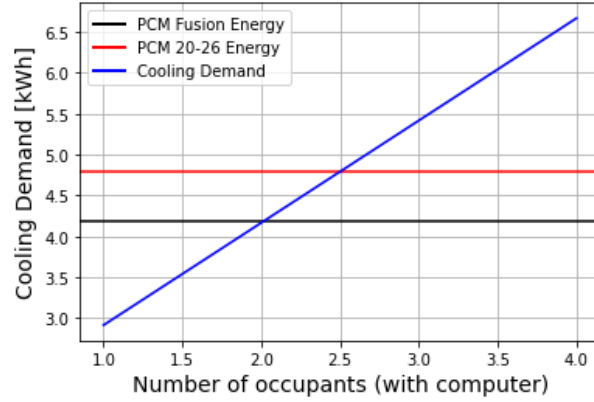


Figure 14: Energy stored in the PCM panels compared with the cooling demand with respect to the number of occupants.

Figure 14 shows that panels with PCM at 20°C can passively withstand the heat load of 2 occupants for a day without having the PCM reaching 26°C . This could show that above 2 occupants, day-active water circulation could be required in order to maintain the operative temperature of the room in an acceptable temperature range (meaning at least Category II as defined in Section 3.1).

5.2.3 Increased Heat Gains

The second scenario will be identical to the first one except that the number of occupants and computers will be increased to 6 each (this scenario will thus be referred as 6OCC). The disposition for the increased heat gains is shown in Figure 15 and the heat gain inputs are listed in Table 9. The goal was to reproduce a realistic disposition of a working room in which 6 people would be working during the whole day.

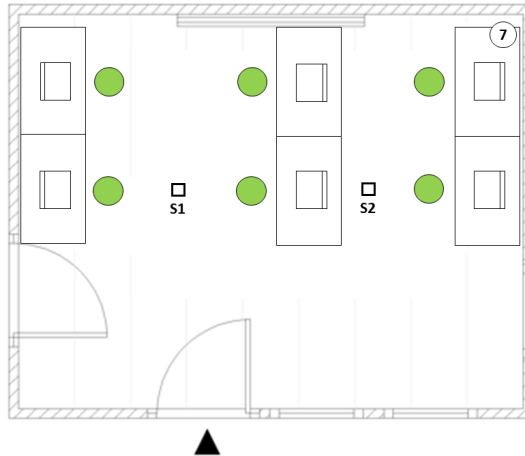


Figure 15: Chamber 6 disposition for the reference scenario (IHG2).

Table 9: Internal heat gains for the 6OCC scenario (IHG2)

Device [-]	Number [-]	Unit heat rate input [W]	Total heat rate input [W]
Lights	2	18	36
Dummies	6	75	450
Computers	6	50	300
TOTAL	/	/	786

The heat gains in that configuration are of 786 W. This is 2.74 times bigger than the previous one. Figure 16 also shows that the solar heat gains account for a much lower proportion in the heat input than in previous scenario (by comparing with Figure 13).

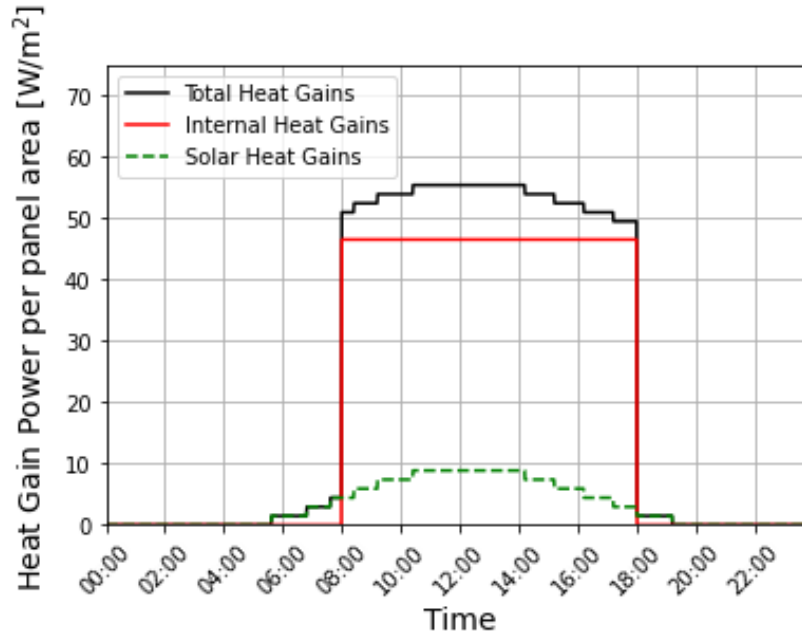


Figure 16: Internal and solar heat gains for the 6OCC scenario (IHG2 and SHG1).

5.2.4 Results

Figure 17 shows that the operative temperature rises much faster during the occupancy for 6OCC. The reference scenario operative temperature peaked around 25°C at 18:00 while the 6OCC scenario had temperatures around 29.2°C at the same hour. This is due to the increased heat gains that generated more heat.

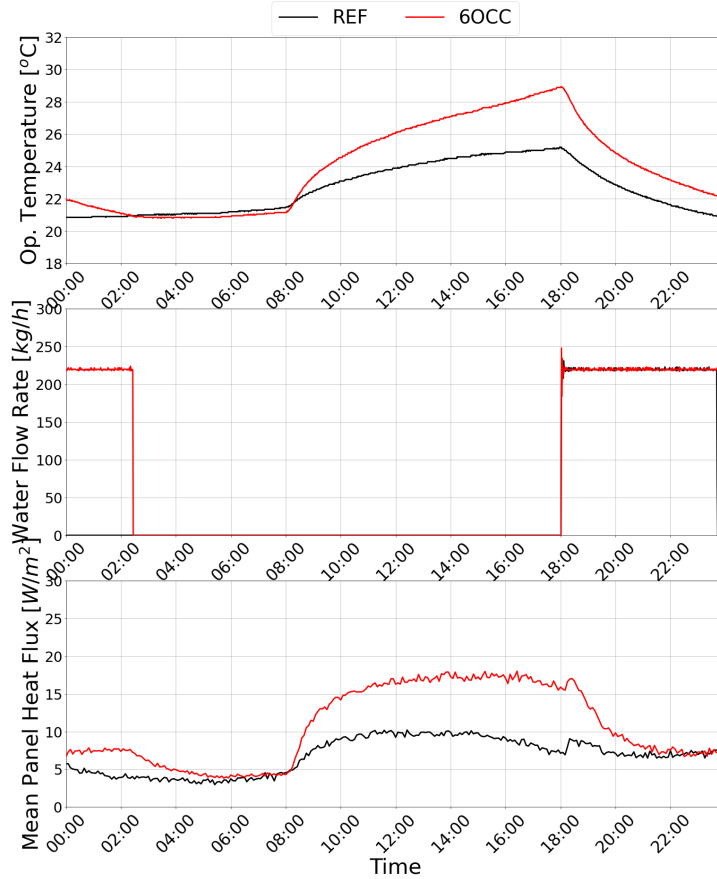


Figure 17: Operative temperature, water circulation flowrate and mean panel heat flux evolution of REF and 6OCC scenarios.

It can also be seen that the water circulation started at 18:00 for both scenarios but ended more than 3 hours later for the 6OCC scenario. This is because more heat was stored in the room and in the PCM at the end of the day, meaning that water had to be circulated for a longer time period to reach the setpoint and discharge the panels.

Moreover, the average panel heat flux was much higher for 6OCC (ranging from 3.8 to 18 W/m^2 with a mean value of 10.7 W/m^2) than for REF (ranging from 3 to 10.2 W/m^2 with a mean value of 6.8 W/m^2). This was expected as the temperature difference between the room and the panels was higher during 6OCC. This difference was due to the increased heat gains and the fact that the panels temperatures had a slower evolution thanks to their higher thermal inertia. This higher temperature difference caused higher heat removal.

In the end, water circulation has been active for about 5h42min a day for the REF scenario and about 8h26min a day for the 6OCC scenario. As said in Section 5.2.3, 2.74 times more heat was generated in 6OCC compared to REF but it took only about 1.48 times more water circulation to extract heat and arrive to similar operative temperatures. This means that the system had a much higher performance in terms of cooling power for the 6OCC scenario (this is shown by the higher panel heat flux and by Figure 18). The system also had a margin of a few hours to recover to the night setpoint in the worst scenario.

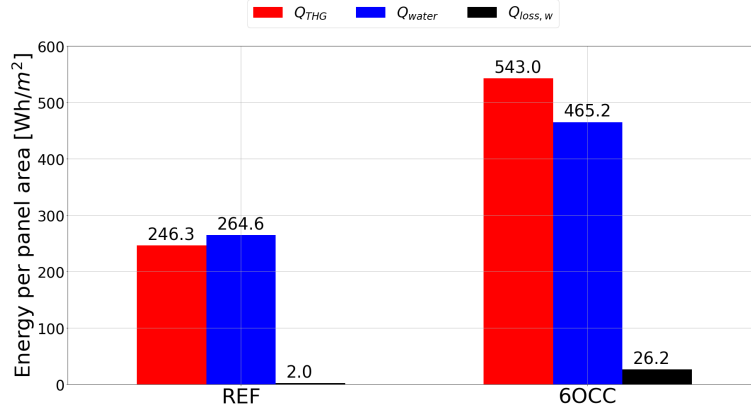


Figure 18: Total heat gains, heat extraction and losses through walls of REF and 6OCC scenarios (over a day).

As shown in at Figure 18, 246.3 Wh/m^2 (of panel area) were generated during the REF scenario and 264.6 Wh/m^2 were absorbed by water circulation. Heat losses through walls are negligible for this scenario (these have been computed using internal and external temperatures of the chamber walls and the walls transmission coefficient present in Section 4.3). This shows the system is able to extract all the heat from the room. The difference between heat input and removal could be explained by sensor imprecision.

During 6OCC, 543 Wh/m^2 were generated and only 465.2 Wh/m^2 were extracted. From this graph, one could conclude that the system is not effective enough to extract all the heat. However, it has been shown that the system can remove all the heat from the room since it stops before the end of the non-occupancy. This gap could be explained by the bigger heat losses that became much less negligible (26.2 Wh/m^2 or in other words 4.8% of total heat gains, explained by the much higher temperatures in the room compared to the lab temperatures), by sensor imprecision, by imprecise heat gain setting or by possible losses through the ground or the ceiling. This also contributed to the greater heat losses. This can also suggest that the operative temperature in the room is getting higher every day. Further investigation is required to determine the origin(s) of this difference.

Finally, Figure 19 shows the distributions of time shares of the operative temperatures in the different thermal categories described in Section 3.1 for both scenarios. The conclusion is that the increase of heat gains had a significant impact on thermal comfort. The thermal comfort goal was Category II, which is the case 77.5% of the time for the REF scenario but only 29.8 % of the time for 6OCC. This shows the need of day-active water circulation to improve thermal comfort.



Figure 19: Comparison of thermal comfort categories time shares of operative temperatures for REF and 6OCC.

5.3 Day-active Water Control and Set-points

Based on results from last section, it was chosen to conduct two experiments with active water circulation. One had an operative temperature day-time setpoint of 25°C (experiment named 25SP). A 25°C setpoint meant that water has been circulated when the operative temperature reached the setpoint value until it reached 24°C . In the other scenario, 23SP, the goal was to obtain a cooler indoor thermal environment and to test the performance of the active heat extraction. Therefore, a day-time setpoint of 23°C was selected. The control strategy using a day-time setpoint and a night-time setpoint for the water circulation is referred to as CTRL2. Other than these setpoint, both scenarios had the same characteristics as 6OCC.

In this part the 6OCC, the 25SP and the 23SP scenarios are compared. One goal is to assess whether day-active water circulation is effective in cooling the room during occupancy. Another is to measure the effect of a lower setpoint.

Experimental measurements for these three scenarios are displayed in Figure 20. A first observation is that day-active water circulation has been very effective in reducing the operative temperature during occupancy compared to the 6OCC scenario. However, even if a difference can be seen between the 23SP and the 25SP scenarios (the damping starts earlier for the 23SP) their curves converge to the same temperature value (26°C) at 18:00. The conclusion is that the system limits in terms of cooling power seem to be reached.

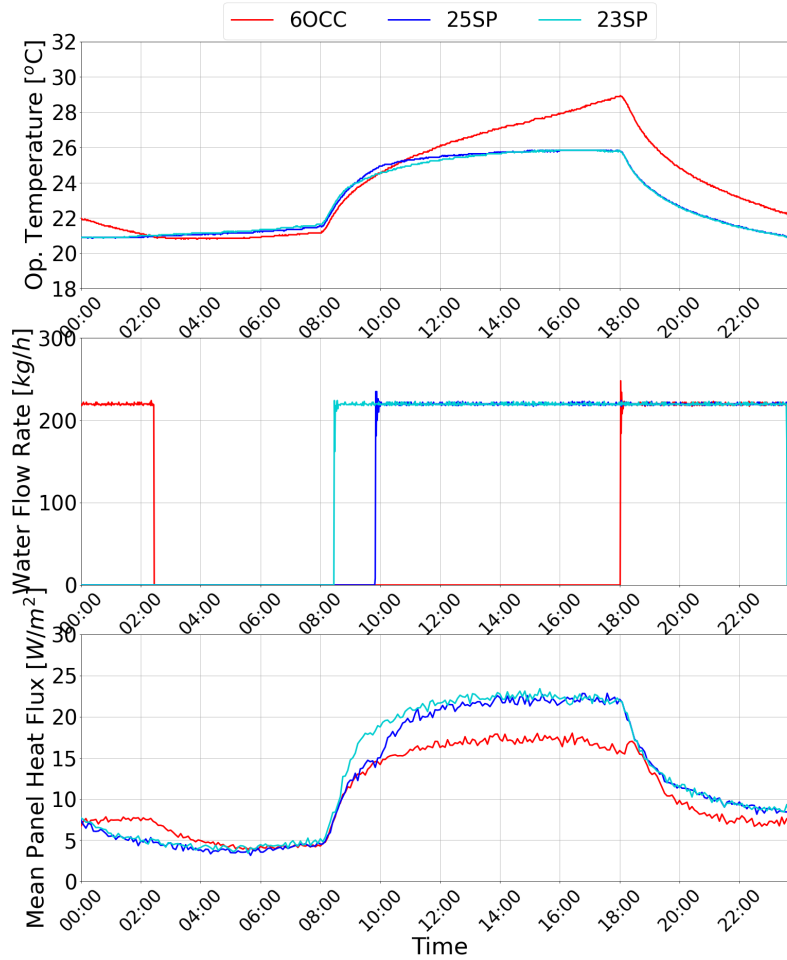


Figure 20: Operative temperature, water circulation flowrate and mean panel heat flux evolution of 6OCC, 25SP and 23SP scenarios.

Looking at the water circulation, the 25SP and 23SP experiments had early starts of water circulation (respectively at 9:51 and 8:28 which are the times the operative temperature reached their respective setpoints) and ended at respectively at 23:39 and 23:35. These contrast with 6OCC scenario that only had night circulation.

The day-active water circulation scenarios had better performance. The 25SP and 23SP scenario heat fluxes range respectively from 3.1 to 22.8 W/m^2 (with a mean of 12.3 W/m^2) and from 3.7 to 23.4 W/m^2 (with a mean of 12.8 W/m^2). This is higher than the values of the 6OCC scenario (range from 3.8 to 18 W/m^2 with a mean of 10.7 W/m^2). This also had to be expected because the panels are directly cooled down by the water, their surface temperatures are thus smaller. On the opposite, the panel surface temperatures of the 6OCC experiment follow the operative temperature more closely.

In the end, the 25SP circulated water for 13h48min (8h09min during the day and 5h39min during the night) and 23SP circulated water for 15h07min (9h32min during the day and 5h35min during the night). Considering the difference in results, the 25 SP scenario showed to be more efficient in this case. These two time periods are however, much longer than the 8h26min of the 6OCC scenario.

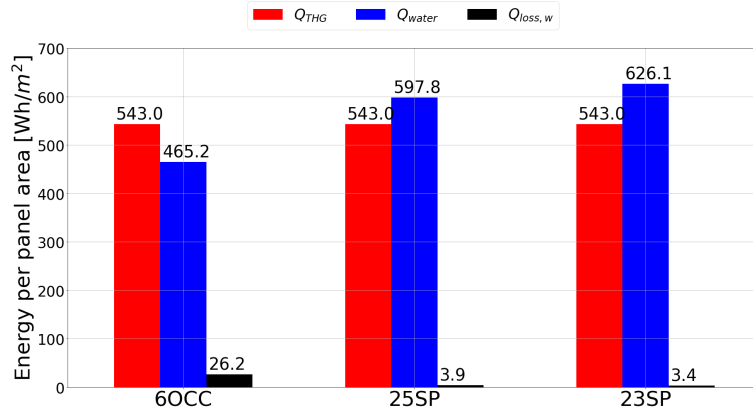


Figure 21: Total heat gains, heat extraction and losses through walls for 6OCC, 25SP and 23SP scenarios (over a day).

Figure 21 shows the results from the panel heat flux graph in Figure 20. Indeed, more heat was extracted during 23SP (626 Wh/m^2) than during 25SP (597.8 Wh/m^2) and even more than for 6OCC (465.2 Wh/m^2). 23SP had water circulating for a longer period of time and thus had more heat extracted than for 25SP. This difference may come from heat losses through the plenum, the slab and the walls as the initial and final temperatures are close for these two scenarios. Indeed, heat losses through walls are smaller when water is circulated. This is partly because the room temperature is lower and thus closer to the lab temperature. Also, as can be seen in Figure 57, the lab temperature was lower for 6OCC than for 25SP and 23SP. This is one of the causes of higher heat losses in 6OCC. The specific heat capacity curve of the PCM could also be in cause (See Figure 3). Indeed, the water was circulated for a smaller amount of time where the partial enthalpy of the material was the highest.

Figure 22 shows the time share of the operative temperatures in the different thermal comfort categories listed in Section 3.1 for the different scenarios compared in this section.

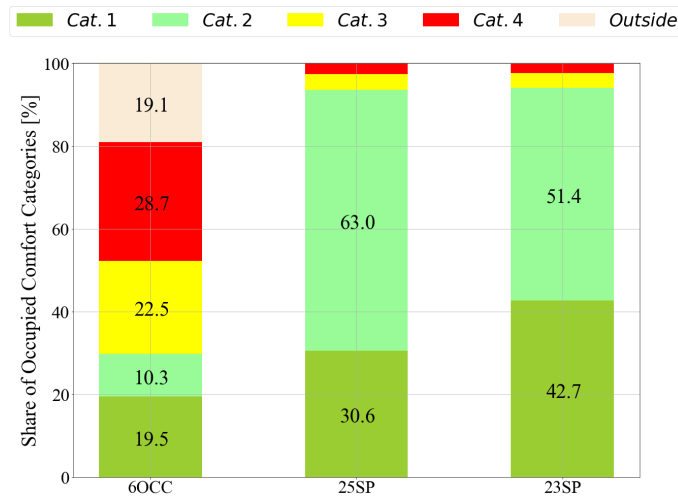


Figure 22: Comparison of thermal comfort categories time shares of operative temperatures for 6OCC, 25SP and 23SP scenarios.

In the Figure above, it can be seen that day-active water circulation had an enormous impact on thermal comfort. Indeed, the time spent at least in Category II went from 29.8% in 6OCC to 93.6% and 94.1% in 25SP and 23SP respectively. These results are even better than the 77.5% of the reference case. The last few percent out of Category II for 25SP and 23SP can originate from a too low temperature at 8:00 (which is between 21 and 22°C because of the night-time setpoint. The water circulation in the 23SP scenario also starts to damp the operative temperature rise sooner causing the latter to stay for a longer period of time in Category I. This shows that day-active water circulation improves thermal comfort even though it uses more water circulation and the share in day-time does not benefit of off-load tariff. The conclusion of this comparison is that the MEPs can be used as radiant panel without ventilation.

5.4 Addition of Ventilation

As mentioned in Section 3.4, the radiant ceiling is not meant to work on its own as indoor air quality requirements have to be satisfied. The 25SPV experiment features a displacement ventilation in addition to the parameters of the 25SP scenario. The ventilation temperature was arbitrarily set to 20°C to avoid discomfort coming from too low temperatures. The flowrate was of 210 m³/h and was computed based on the method based on perceived air quality described in Section 3.2. During non-occupancy, using dimensions from Section 4.3 (considering the chamber volume under the ceiling), it has been computed that at least 30.62 L/s has to be supplied to the chamber for the two hours prior to occupancy.

Figure 23 shows that the ventilation with the previously mentioned settings was able to cool the room without day-active water circulation with the 25°C setpoint. Indeed, the temperatures always stayed below 25°C during the day. A small spike at 18:00 happened because the ventilation stopped and the water circulation needed some time to become effective. This time may be the time required to cool down the panels (especially their surface).

The water circulation still operated during the night in order to cool the room down and the panels still had a non negligible cooling effect during the day (having mean panel heat flux ranging from 3.2 to 12.5 W/m² with an average of 7.6 W/m²).

However, this remains small compared to the effect of ventilation that removed up to 31.4 W/m² (per panel area). The ventilation heat removal per panel area has been computed using the air density ρ_a ($= 1.3 \text{ kg/m}^3$), the air specific heat cp_a ($= 1000 \text{ J/(kg} \times \text{K)}$), the air volumetric flowrate \dot{V}_a as well as its return and supply temperatures ($T_{r,a}$ and $T_{s,a}$) as in Equation 4:

$$\dot{Q}_{vent,m^2} = \rho_a \times cp_a \times \dot{V}_a \times \frac{(T_{r,a} - T_{s,a})}{A_{ceil}} \quad (4)$$

For the 25SPV scenario, the water circulation started at 18:00 and ended at 00:18. This account for 6h18min which is very small compared to the 13h48min of the 25SP. This is still to be expected as the radiant ceiling is not the only mean of cooling in the 25SPV scenario. A conclusion can be drawn from the fact that the water circulation happened only during non-occupancy, the panels behaved like a TABS system in 25SPV.

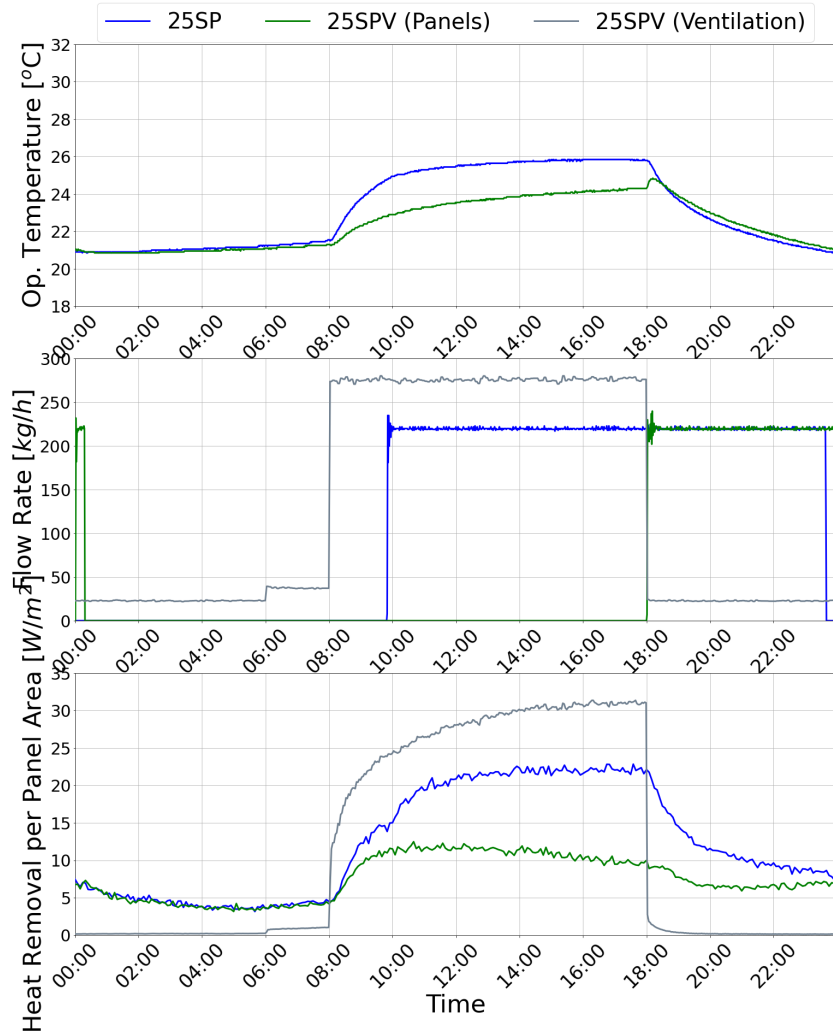


Figure 23: Operative temperature, water circulation flowrate and heat removal per panel area evolution of 25SP and 25SPV scenarios (operative temperature is common to the two technologies for 25SPV).

Figure 24 shows the heat gains, heat extraction via the water circulation and the ventilation and heat losses through walls for 25SP and 25SPV scenarios. It shows that the heat removal of ventilation is actually lower than the effect of the ceiling panel for 25SPV. However, it is far from negligible as these two values are almost even. In the end, the 25SPV had a total heat removal of 579.3 Wh/m^2 using both ventilation and the radiant ceiling which is comparable to the 597.8 Wh/m^2 of the 25SP scenario. As the temperatures were kept low during the whole scenario, not much heat losses were experienced in 25SPV.

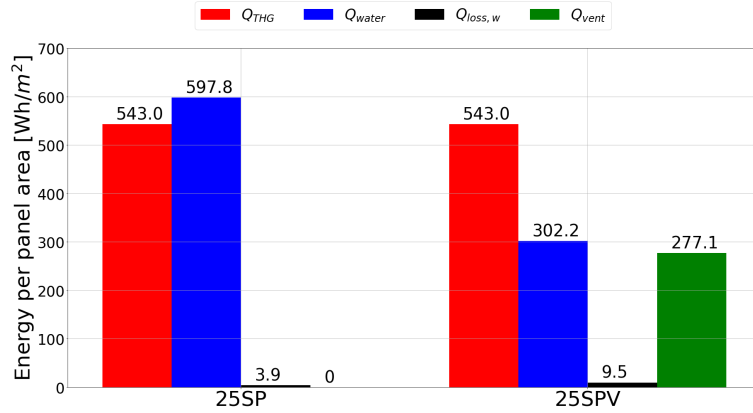


Figure 24: Total heat gains, heat extraction and losses through walls for 25SP and 25SPV scenarios (over a day).

Looking at Figure 25, one can see that the ventilation with the chosen parameters did not have a good impact on thermal comfort. Even though the share of time the operative temperature in Category I doubled and went to more than 60%, the share of time in at least Category II went from 93.6% down to 78.7%. By looking at Figure 23, it is clear that the ventilation damped the operative temperature rise too much and the temperatures were thus too low during the beginning of the occupancy. This is the main cause of the decrease in thermal comfort mentioned above.

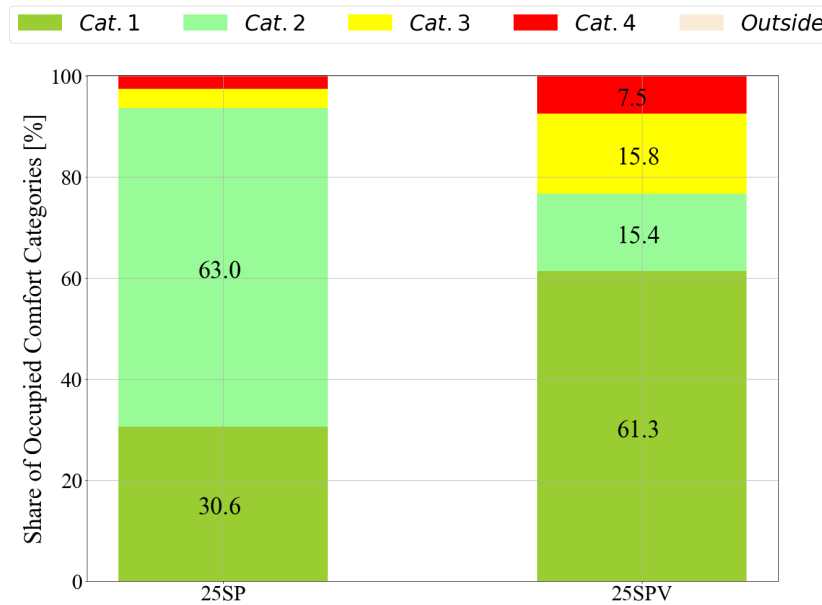


Figure 25: Comparison of thermal comfort categories time shares of operative temperatures for 25SP and 25SPV scenarios.

5.5 Recovery Scenario

Now that day-active water circulation and ventilation have been introduced, one thing that could be interesting to determine is whether the system with the radiant ceiling and the ventilation is able to extract more heat than what it generated with the heat gains.

The 3PM scenario aimed to start the radiant ceiling near the end of the occupancy. As the name suggests, the water circulation started at 3PM, in the second half of the occupancy period (this has been referred to the CTRL3 control strategy). The day water circulation setpoint has been put to 23°C for the water circulation to work. Note that the night water circulation has been put to 24°C to limit the use of the water circulation during the night and let the system heat up. The ventilation was working as in the 25SPV scenario without interruption. One goal of this scenario was to assess the resilience of the system if an unexpected event happened (e.g. system failure). Another was to assess if the system was able to remove more heat than what the heat gains generated, having thus a tight control on the operative temperature. As this case was very specific, it was not compared to another scenario.

In Figure 26, it can be seen that the system behaves like in the 25SPV scenario at the beginning of the day. When 15:00 is reached, the operative temperature in the room is 24.7°C . Then water circulation starts and the operative temperature starts to drop until 18:00 when it reached 24°C . Because of this temperature value, the water circulation and the ventilation stopped together at 18:00. The water circulation was thus active for only 180 min and kept the temperatures below 24.7°C . One can also see that even with the active water circulation, the ventilation kept a major role in heat removal during occupancy.

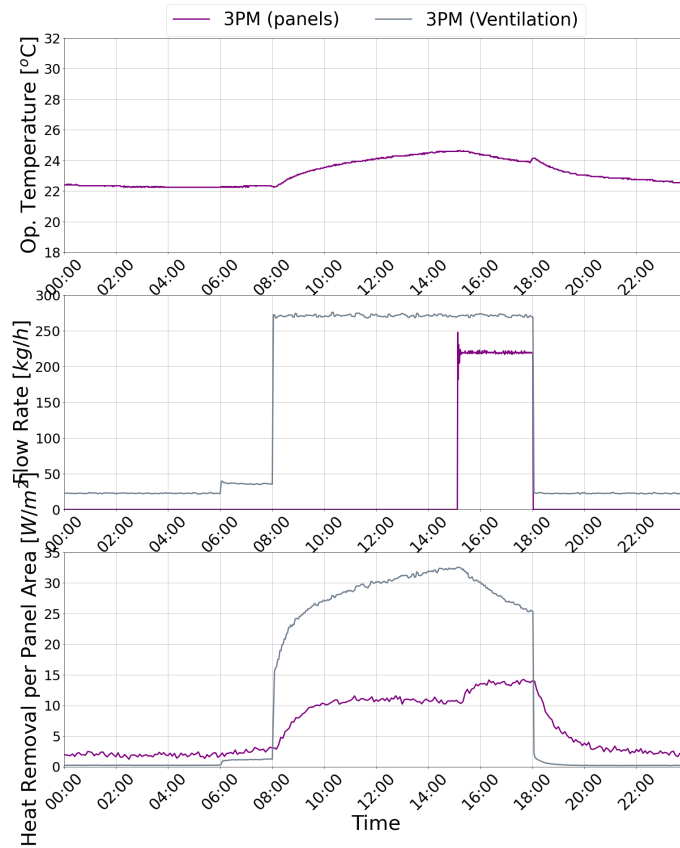


Figure 26: Operative temperature, water circulation flowrate and heat removal per panel area evolution of the 3PM scenario (operative temperature is common to the two technologies).

It is also noticeable that the ventilation was again dominant during occupancy in heat extraction as it extracted up to 33 W/m^2 (per panel area) of heat whereas the ceiling extracted in a range from 1.2 to 14.3 W/m^2 with an average of 6.2 W/m^2 during the scenario. However, the system as whole was able to extract a good amount of heat at once (up to around 45 W/m^2).

5.6 Attempt of Tight Control

The goal of the TIGHT scenario was to have a very tight control on the room operative temperature while lowering the impact of the ventilation. This is why the ventilation temperature has been set to 22°C . Also, the flowrate during occupancy was lowered to $152 \text{ m}^3/\text{h}$ by using the value from the method using limit values of substance concentration detailed in Section 3.2. The attempt of tight control consisted in having the most constant operative temperature possible. This is why both of the day and night operative temperature setpoints were set to 23°C . This scenario has been compared to the 25SP as the baseline.

As can be seen in Figure 27, even though the operative temperature of the TIGHT scenario starts around 1°C warmer than the one of the 25SPV, both temperatures end up at similar values at the end of the day. We can thus expect more heat to be extracted during the TIGHT scenario.

Looking at the use of water circulation, it was used for 12h36min during the TIGHT scenario which is twice the time of the use in the 25SPV scenario. This can be explained by the reduction of the effect of ventilation as mentioned above (that can also be seen in Figure 27 by looking at the flowrates). Even though ventilation was present, the panel system was still able to absorb heat in a range from 3.5 to 20.7 W/m^2 with an average of 11.4 W/m^2 , leading the total system to extract up to 34 W/m^2 consistently during the day.

Something noticeable is that in the TIGHT scenario, water circulation was mostly used during occupancy (9h45min in contrast with 2h51min outside occupancy for a total of 12h36min) whereas 25SPV used its water circulation during the night only. This can be explained by the choice of the different setpoints and the ventilation parameters. Thus, these parameters and setpoints are very important in determining if the panels behave similarly to a TABS system or to a radiant panel.

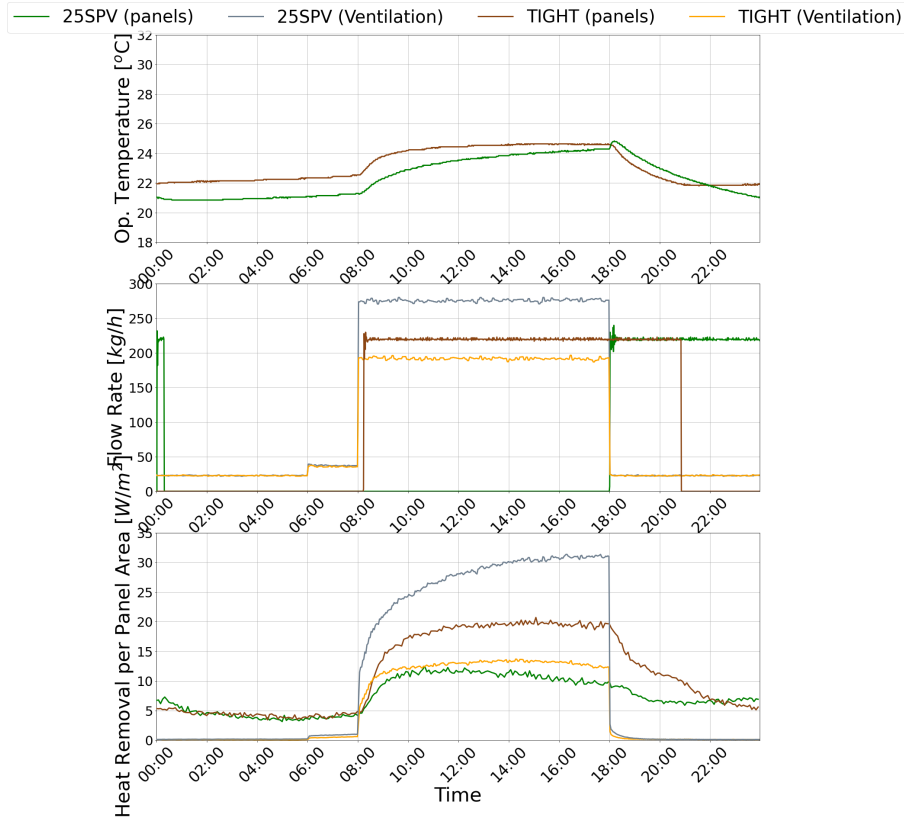


Figure 27: Operative temperature, water circulation flowrate and heat removal per panel area evolution of 25SPV and TIGHT scenarios (operative temperature is common to the two technologies for both scenarios).

Figure 28 confirms that more heat was extracted in total during the TIGHT scenario than during the 25SPV one (685.4 Wh/m^2 per panel area for the first and 579.3 for the second). The goal of reducing the cooling impact of the ventilation was fulfilled as the second value of Q_{vent} is about 46% of the first. The radiant ceiling became thus more present in TIGHT. In 25SPV, the water loop and the ventilation extracted respectively 52.2 and 47.8% of the heat. In TIGHT, these proportions changed respectively to 81.4 and 18.6%

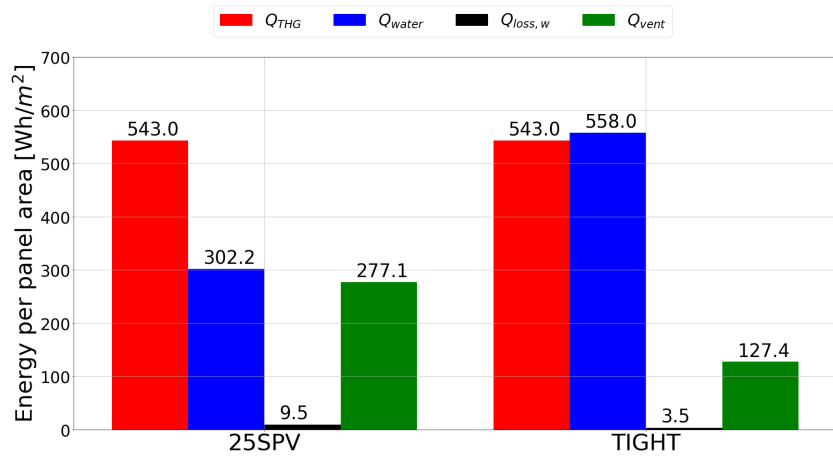


Figure 28: Total heat gains, heat extraction and losses through walls for 25SPV and TIGHT scenarios (over a day).

Finally, Figure 29 shows that with a good control strategy, the system is able to provide excellent thermal comfort by still using the ceiling as main heat extraction. The operative temperature stayed in Category II during 95.8 % of the time including 92.1% in Category I. The 4.2% in Category III are still due to the slightly low temperatures at the beginning of the occupancy.

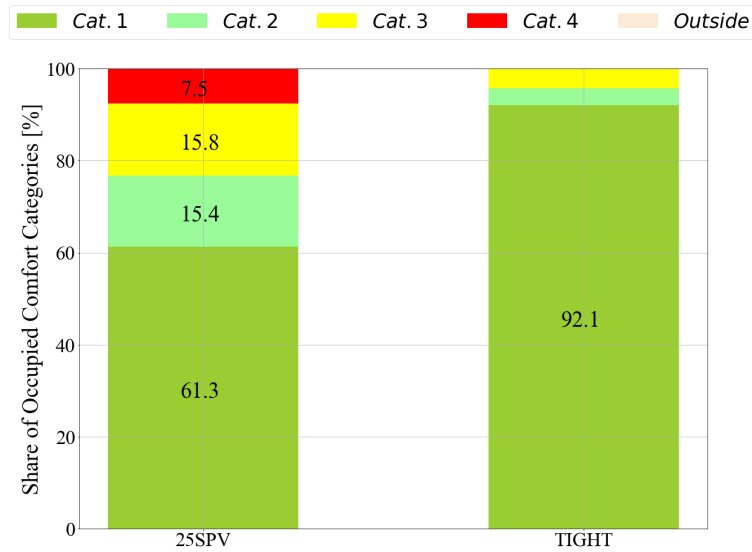


Figure 29: Comparison of thermal comfort categories time shares of operative temperatures for 25SPV and TIGHT scenarios.

5.7 Discussion

Figure 30 summarises all thermal comfort categories distribution presented in this investigation. It shows that addition of heat gains had a very negative impact on thermal comfort. Addition of ventilation and/or day-active water circulation was thus necessary. By introducing day water circulation (6OCC to 25SP), it was possible to improve comfort a lot (from 29.8% to 93.6 % of the time in Category II) at the cost of more water circulation and to play on the proportion inside Category I by adjusting setpoints (25SP to 23SP). However, a comparison between results of 25SP and 23SP showed that the system had limits in heat removal and thus on performance with the chosen parameters in this study. As a matter of fact, 23SP failed to maintain the operative temperature close to its setpoint even if the thermal comfort was still improved. 25SPV showed that ventilation could have negative impact on thermal comfort if its parameters (flow rate, inlet temperature) were not well set. The radiant ceiling was still extracting more heat on a whole day period but was dominated by the ventilation during occupancy. The effect of the ventilation did not allow day-active water circulation and the radiant ceiling followed the classical TABS control. The TIGHT scenario showed that by adjusting the setpoints and by reducing the impact of ventilation (lowering the flow rate and/or increasing the inlet ventilation temperature), it was possible for the MEPs to behave as a radiant ceiling. It also showed that a very tight control on the operative temperature was possible, providing an excellent thermal comfort.

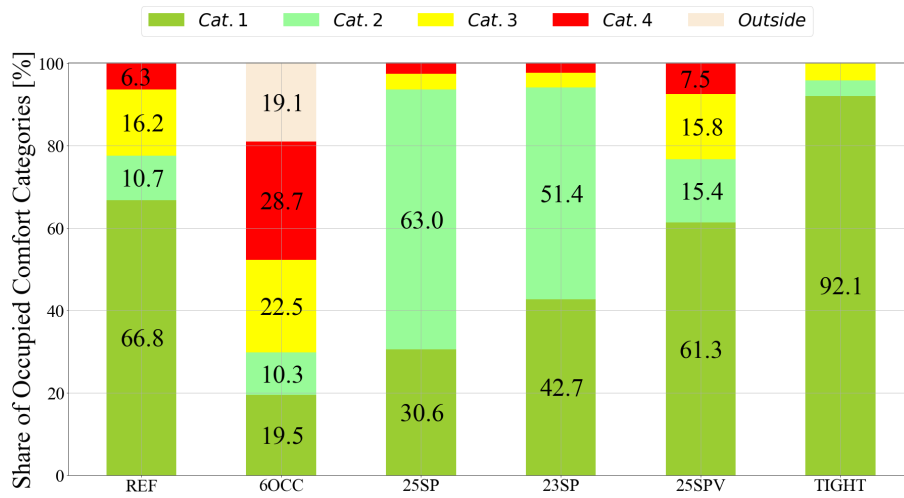


Figure 30: Comparison of thermal comfort categories time shares of operative temperatures for all scenarios.

Table 10 summarises relevant results regarding heat extraction for all scenarios. It highlights that increasing heat gains (from REF to 6OCC) increases the heat extraction rate of the panels as it creates a higher difference between operative temperature and panel surface temperature. By adding water circulation (25SP and 23SP), the heat extraction and the thermal comfort increase but these come with a cost of intense day-active water circulation. The water still has to circulate during non-occupancy to cool the panels afterwards. Changing the day setpoint as in 23SP compared to 25SP did not induce a significant gain in performance as the system limits were reached. Adding ventilation with parameters mentioned in Section 5.4 (25SPV) reduced heat extraction of the panels as the ventilation had a dominant impact during occupancy. The impact was high enough to prevent the day setpoint to be reached as thus no water was circulated during the day. Tuning the setpoints and the ventilation

parameters as in TIGHT allowed the panels to extract almost as much heat as if the ventilation was not active. This with the advantage that ventilation provided enough fresh air to limit the accumulation of CO₂ and a non-negligible heat extraction. A further study could be to investigate the energy use of such as scenario and refine the choice of the parameters to improve energy efficiency and cost of operation of the system without compromising on thermal comfort.

In case of water system deactivation for a part of the day (3PM), the results showed that the system could reach high performance especially thanks to ventilation. A further study could be to investigate this type of scenario using a ventilation with less impact.

Table 10: Summary of relevant results regarding heat extraction for all scenarios (specific values are provided relative to panel surface area).

Scenario	REF	6OCC	25SP	23SP	25SPV	3PM	TIGHT
Use of water circulation (D N) [h:m]	0 5:42	0 8:26	8:09 5:39	9:32 5:35	0 6:18	5:00 0	9:45 2:51
Panel [Min,Max] and Average Heat Extraction Rate [W/m^2]	[3,10.2]	[3.8,18]	[3.1,22.8]	[3.4,23.4]	[3.2,12.5]	[1.2,14.3]	[3.5,20.7]
	6.8	10.7	12.3	12.8	7.6	6.2	11.4
Mean Ventilation Heat Extraction Rate (Occupancy) [W/m^2]	/	/	/	/	27.2	28.3	12.43
Total System Maximum Heat Extraction Rate [W/m^2]	10.2	18	22.8	23.4	43	45	34
Heat Extracted by circulated water [Wh/m^2]	264.6	465.2	597.8	626	302.2	/	558
Heat Extracted by ventilation [Wh/m^2]	0	0	0	0	277.1	/	127.4

Table 11 shows mean panel heat flux values depending on whether the room is occupied and whether water circulation is active. First focusing on non-occupancy, it shows that heat fluxes are consistently higher when water circulated for all scenarios. Moreover, a comparison can be done between the mean heat flux value of occupancy without water circulation of 6OCC and the mean heat flux values of 25SP, 23SP and TIGHT (during occupancy). The former is always smaller than the others, even if the operative temperatures in the 6OCC scenario were more extreme. The conclusion that can be drawn is that circulating water in the MEPs improves their heat absorption as the heat is able to bypass the PCM through the aluminum structure. Without ventilation, this improvement is of about 35%.

Table 11: Mean panel heat fluxes for various conditions for all scenarios [W/m^2].

Scenario	REF	6OCC	25SP	23SP	25SPV	3PM	TIGHT
Occupancy / Water Circulation	/	/	21	20.8	/	13.2	18.1
Occupancy / No Water Circulation	8.8	15.4	10.3	6.2	10.5	9.8	4.8
Non-Occupancy / Water Circulation	7.3	9	11.7	11.7	7	14	13.2
Non-Occupancy / No Water Circulation	4.1	4.9	4.6	4.9	4.3	2.9	5.1

6 Introduction to Finite Element Method

Simulations are an important part of an investigation because they enable to explore scenarios that would be time and cost effective (or impossible) to do in an experimental setup. Many simulation tools exist for each engineering domain. Phase Change Materials (PCM) in buildings make no exception and can be simulated using tools such as TRNSYS, EnergyPlus, EES and many others. Finite Element Method (FEM) is one of the most precise tools out of them. However, this precision comes with a cost which is heavy computation. This is why this investigation will use FEM as a way to evaluate simpler and more flexible models that could be inserted in other tools such as TRNSYS and EnergyPlus.

This section aims to introduce the Finite Element Method, its benefits and its different uses especially concerning PCMs and radiant systems.

6.1 Brief Description of the Method

FEM (Finite Element Method) is a tool part of computational mechanics. It consists in the discretization of complex continuous geometries into simpler finite structures (called finite elements) in order to solve theoretical and simple equations on each element (divide and conquer approach). Constraints between elements are added to ensure continuity. All solutions are then put together to obtain a geometry dependent results of the complex structure. Figure 31 shows an illustration of this process.

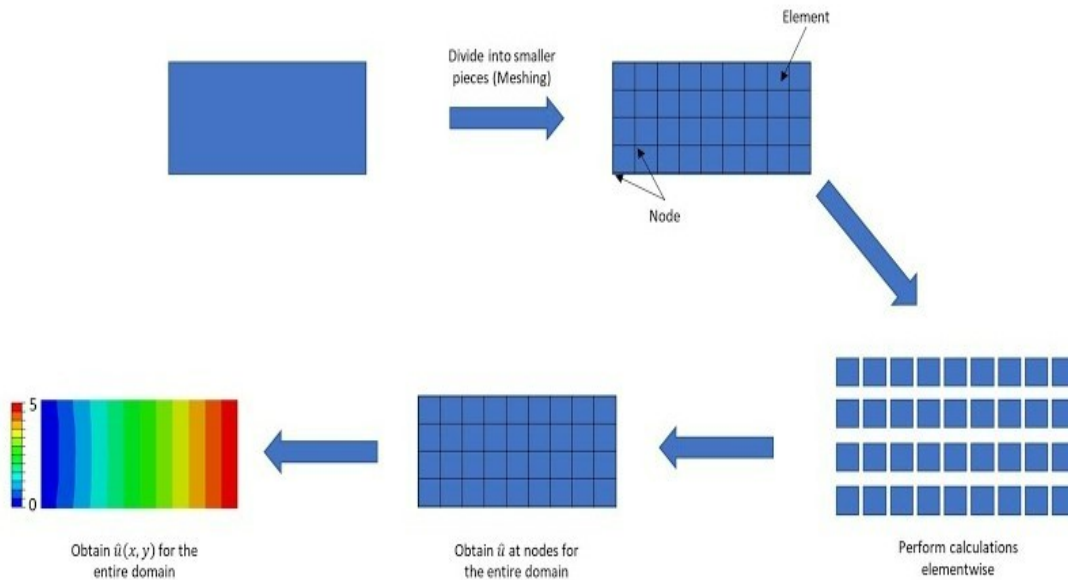


Figure 31: Representation of the basic concepts of Finite Element Method [39].

This method requires many steps:

- 2D or 3D modelling of the structure: done in a modelling software, this step defines the geometry of the problem.
- Meshing of the structure: done using a modelling software and a meshing solver, this step defines how the geometry will be discretized and allows to apply material properties to the model.

- Definition of the constraints and the loads related to the simulated model: done using a simulation solver, this step defines the physical problem.
- The simulation: Run in either steady-state or transient time consideration using a solver, this step performs iterative processes. If the previous steps are done in a way that the problem is well-defined, the solver can converge and yield a solution.

The modelling software and the solver (for both meshing, simulation definition and solving) used in this thesis are respectively **Siemens NX 11** and **Simcenter Thermal/Flow**.

6.2 Advantages of the Method

Finite Element Method has many advantages:

- It can solve problems having a complex geometry that could not have analytical solutions.
- It allows to study complex material behaviour (for example, phase change).
- It allows to get results without making experiments that are not feasible or too expensive.
- The simulations present an adjustable trade-off between precision and computational time with possible adjustment.
- It displays geometry-dependent results inside the structure where a sensor couldn't be introduced without creating a perturbation in the system.
- It can be applied to lots of engineering problems (frequently used in aeronautics, biomedical engineering, civil engineering, automotive, etc). Examples are shown in Figure 32.
- It can simulate complex loads (space-wise and time-wise).

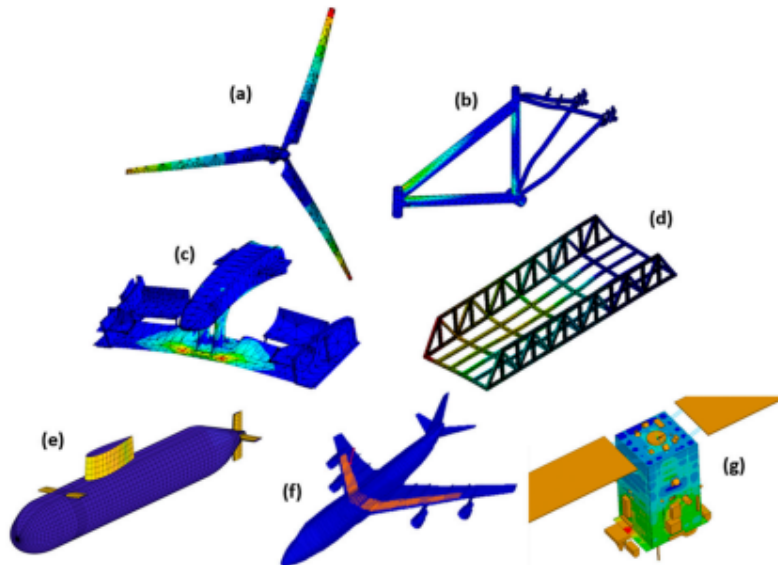


Figure 32: Examples of FEM applications aiming to study polymers [40].

FEM is thus a very powerful tool. However, the results that the computer yields could be inconsistent even if a solution exists. In fact, this method implies some hypotheses (simplification of geometry and of material behaviour, polynomial assumption of field values inside an element, other assumptions are related to the solving techniques). Critical analysis and/or validation of the results are thus very important.

6.3 FEM-Linked Bibliographic Review

Finite Element Method has been used in lots of different domains (see previous subsection). Thermal and/or flow models can also be relevant in order to investigate and optimize the performance of radiant systems.

This has been the case since a few decades. In 2006, Sattari et. al. [41] studied the effect of pipe parameters (such as spacing, radius, type), of the storage material and of the radiative cover for a radiant floor.

Other more recent uses of FEM are also directly focusing on PCM materials themselves. For example, a study has been done by Feng et. al [11] to investigate the effect of introduction of nanoparticles inside a PCM layer in order to enhance its thermal conductivity.

Furthermore, the consideration of the systems' geometry allows to optimize simple existing structures [10]. It can also lead to the elaboration of models of more complex matrices that can then be combined with PCM [42].

Finally, given the precision but also the complexity of these models, lots of studies aim to create simpler models that return comparable results to FEM ones in order to reduce the computation time and complexity. An example of that kind of study has been done by Kilkis et. al. [43]. This could be useful to integrate the simpler panel model in a more complex simulation (for example, not only focusing on the panel but on a whole room/building).

7 Presentation of the Model

This section aims to present the Finite Element model of the panel. This includes the assumptions, the geometry, the choice of meshing size and the definition of the simulations' conditions.

7.1 Geometry and Materials Definition

The first assumptions of this model are made on its geometry. In fact, starting from a real panel's geometry (shown in Figure 33), it is possible to find a symmetric redundancy.

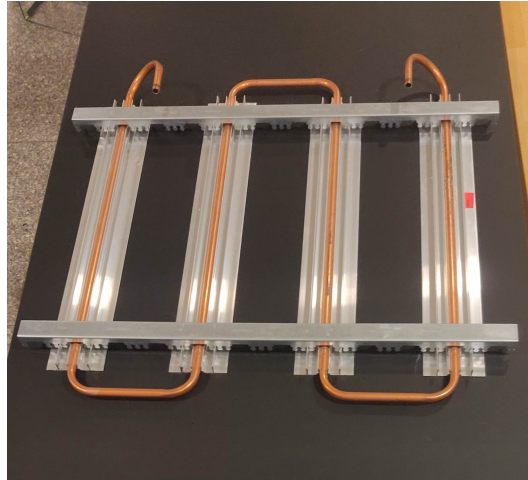


Figure 33: Picture of a pipe profile.

From this redundancy and by measuring the panel dimensions, a 2D model representing one aluminium fin with a pipe was made. These assumptions were made in order to simplify the problem and to reduce the computation time. The materials of the different parts of the model are given in Figure 34. These were assigned during the meshing but were shown here for readability reasons. The model is 150 mm wide (corresponding to the pipe spacing) and as thick as a panel (29 mm : See Figure 5). Note that the model still presents a symmetry (vertical axisymmetry in the middle of the model) and could have been halved again. It was not done for representation reasons and because it was considered efficient enough. Drawings with main cotes are available in Appendix C.

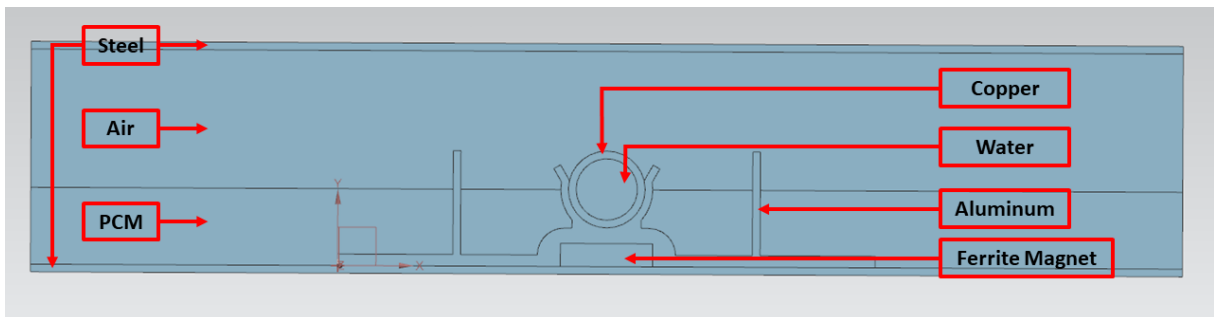


Figure 34: 2D model of a fin with materials description.

The PCM layer has been subdivided into three sub-layers of same height in order to make an investigation on PCM vertical stratification. This study can be found in Section 9.5.

The materials properties come from diverse sources. First, Siemens NX12 provides a library for commonly used materials. The list of these materials with their main characteristics can be found in Table 12:

Table 12: Materials used from the NX library for the model and their characteristics.

Material	Name in NX12	Density	Heat Capacity	Thermal Conductivity
[/]	[/]	$\left[\frac{kg}{m^3}\right]$	$\left[\frac{kJ}{kg \times K}\right]$	$\left[\frac{W}{m \times K}\right]$
Aluminium	Aluminum6061	2711	0.896	173.3
Copper	CopperC10100	8920	0.385	387
Ferrite	Iron Malleable	7358	0.447	51.06
Steel	Steel	7829	0.434	43.74

The two fluids (air and water) were not in the library as for this type of simulation only solids are expected. So common values have been used for these materials (see Table 13).

Table 13: Materials used from the NX library for the model and their characteristics.

Material	Density	Heat Capacity	Thermal Conductivity
[/]	$\left[\frac{kg}{m^3}\right]$	$\left[\frac{kJ}{kg \times K}\right]$	$\left[\frac{W}{m \times K}\right]$
Water	1000	4.196	0.598
Air	1.2	1	0.02

The characteristics for the phase change material (Rubitherm24) have already been listed in Section 4.1.

7.2 Model Assumptions

The model is based on the following assumptions:

- As said before, a first assumption was made on the geometry. The model is 2D and represents one aluminium fin.
- The model is purely thermal (a thermal/flow model shall be 3D and it increases a lot the meshing and computation time). This means that the different fluids (air, water and liquid phase PCM) are considered as non-moving solids. Whereas the air and the PCM are not intended to move, this hypothesis for water requires to define a heat transfer coefficient (h_W) to the copper pipe. The latter is computed using the following equation [45] :

$$R_W = \frac{W^{0,13}}{8,0 \cdot \pi} \left(\frac{d_a - 2 \cdot s_r}{\dot{m}_{H,sp} \cdot l} \right)^{0,87} \quad \text{and} \quad h_W = \frac{1}{R_W} \quad (5)$$

Where:

- R_W is the wall resistance between the water and the copper pipe.
 - W is the pipe spacing.
 - d_a is the outer pipe diameter.
 - s_r is the pipe thickness.
 - $\dot{m}_{H,sp}$ is the water flowrate.
 - l is the pipe length (assumed to be 1 m as the model is 2D).
- The density of the phase change material is constant. It has been assumed to be the average of the liquid and solid phases densities.
 - Materials have a constant thermal conductivity with respect to temperature.
 - There is no contact resistance between the different elements of the model.
 - The operative temperature will be considered as the ambient temperature for the radiative and convective heat transfers with the lower steel plate.
 - The convective heat transfer coefficient between the panel and the room (h_c) is computed using the following ASHRAE correlation for ceiling cooling [46] (T_s and T_a being respectively the panel surface temperature and the air temperature).

$$h_c = 2.13 \cdot |T_s - T_a|^{0.31} \quad (6)$$

- No heat transfer is considered for the upper steel plate. This assumption could be justified by the layer of air acting as an insulator between the PCM and the plenum.

7.3 Meshing and Choice of Element Size

As explained in Section 6.1, the meshing part defines the discretization of the model. An important parameter is thus the element size (i.e. characteristic size) of the different meshes. This parameter is determinant for the trade-off between precision and performance. The element size doesn't have to be constant in a model. It can be tuned depending on the size of smallest elements of the geometry and/or on the will of result precision in that same area.

A common good practice when using finite elements is to vary the size of the elements in order to determine the effect of their size on results and on computation time and to see if there are singularities. These are locations in the model in which some variables could tend to infinite values although a solution is given, they originate mainly from bad meshing.

For this, a simple steady-state analysis was made on the previously defined model with smallest element size varying between: $[0.2, 0.3, 0.5, 1, 2] \text{ mm}$. The smallest element size will be applied to the following parts of the model (See Figure 35):

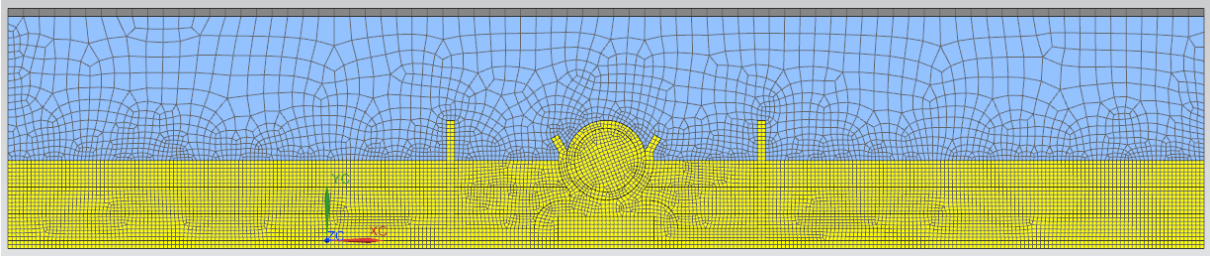


Figure 35: Minimum element size area definition (in yellow).

The parameters of the steady-state simulation are the following:

- Water temperature set to 18°C .
- Ambient air temperature set to 24°C .
- Radiation of the bottom face of the panel with the ambient with an effective emissivity of 0.85 (as the bottom plate is made of steel [44]).
- Convection coefficient of the bottom face of the panel with the ambient of $2.3 \frac{\text{W}}{\text{m}^2}$ (arbitrarily chosen plausible value, details of this computation in Section 7.2).
- Heat transfer coefficient between the water and the copper pipe of $190 \frac{\text{W}}{\text{m}^2}$ (arbitrarily chosen plausible value, details of this computation in Section 7.2).

The temperature distribution at steady-state for the simulation with 0.5 mm elements is shown in Figure 36 :

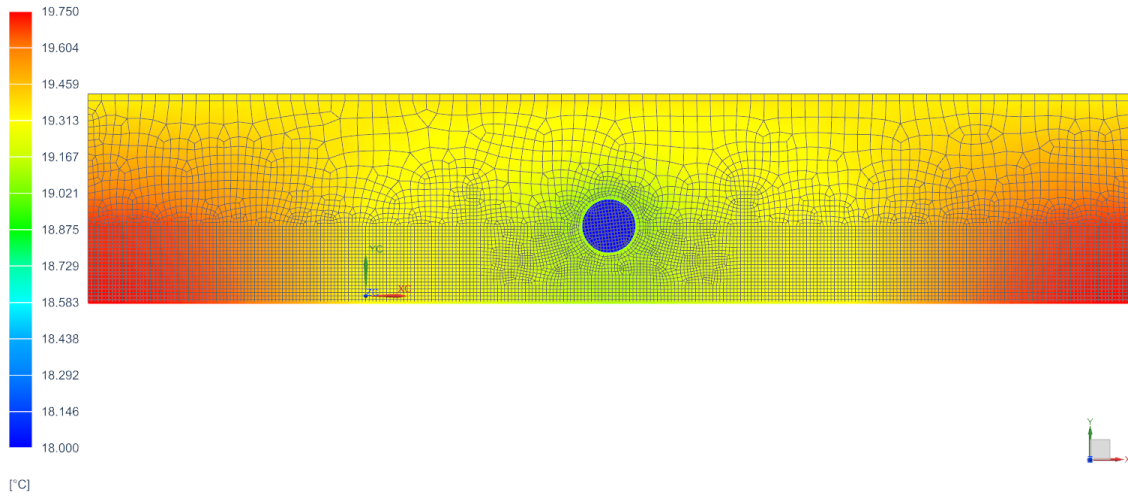


Figure 36: Temperature distribution in the panel for a steady-state simulation (in $^{\circ}\text{C}$).

From Figure 33, one can deduce that the panel center temperature corresponds to the temperature in the left or right bottom side of the model. Figures 37 and 38 show the evolution of the computation time and the panel center temperature with respect to element size:

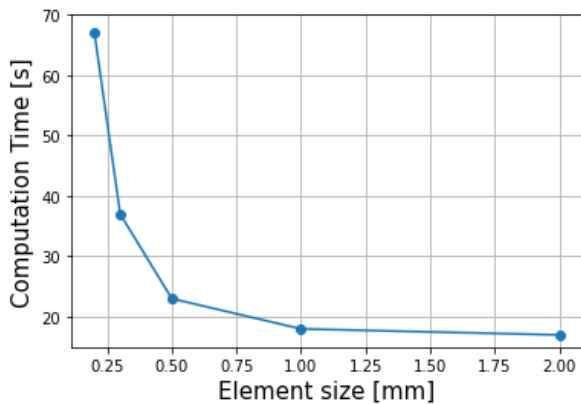


Figure 37: CPU time with respect to minimum element size.

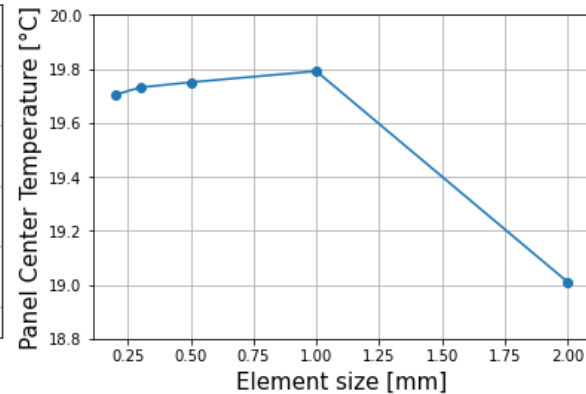


Figure 38: Panel center temperature with respect to minimum element size.

When the size of the elements decrease to less than 0.5 mm , the computation time significantly increases due to a substantial growth in the number of computation points involved. Furthermore, when the elements are larger than 1 mm , the precision of the temperature solution decreases by about 0.8°C . This could be explained by the geometry of the model because some parts of the fin are 1 mm thick. The elements are thus bigger than the geometry and cause a decrease of solution quality. For the next investigations, we will use a smallest element size of 0.5 mm as not a lot of precision is to be gained with smaller element size considering the increase of computation time.

7.4 Simulation Definition

Now that the model and the mesh have been defined, only the simulation constraints and parameters remain. The model was validated using the reference scenario (detailed in Section 5.2.1). From the description of that scenario, two cases can be distinguished:

- **Non-Occupancy: from 6 pm to 8 am.** Where the water is being circulated in the panel to cool it down. Then, when the room reaches the temperature setpoint (21°C), the water circulation stops and the panel will only exchange heat with the room.
- **Occupancy: from 8 am to 6 pm.** Where the panel is initially cold because of the water circulation and will then heat up because of the heat gains generation during the day. In this time range, no water circulation occurs through the pipe profile.

Non-Occupancy Simulation

This simulation has the following parameters and boundary conditions. Some of these are represented in Figure 39:

- The software simulates 14 hours of behaviour with a 1 minute time step and result sampling rate.
- The specific heat of the PCM is the one in the cooling direction. This could lead to small imprecision when the water circulation will stop as the panel will heat up.
- The water-copper heat transfer coefficient, the convection and the radiation parameters are defined and/or computed for every minute using the assumptions of Section 7.2 using experimental data.
- The water temperature, ambient temperature and initial model temperature are set to identical values as the experimental data (depending on time except for the latter). The initial temperature value will be the measured panel surface temperature at the beginning of the scenario.

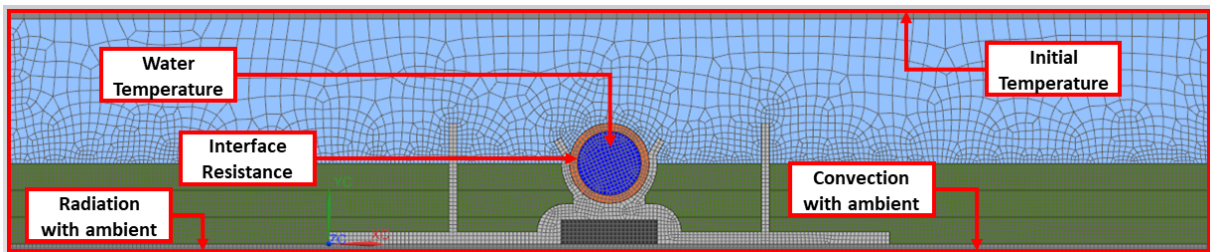


Figure 39: Non-occupancy simulation boundary conditions.

Occupancy Simulation

The simulation parameters and boundary conditions must also be defined. Some are similar to the previous case's one and are represented in Figure 40:

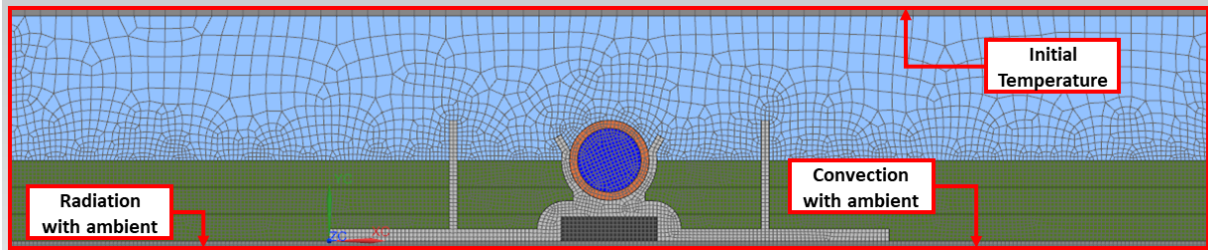


Figure 40: Occupancy simulation boundary conditions.

- The software will simulate 10 hours of behaviour with a 1 minute time step and result sampling rate.
- The specific heat of the PCM is the one in the heating direction. This time, the behaviour of the PCM will not change as the panel will only heat up during the considered scenario.
- As there is no water circulation, the water temperature will evolve freely.
- The convection and the radiation parameters are still defined and/or computed for every minute using the assumptions of Section 7.2 using experimental data.
- The ambient temperature and initial model temperature are still set to identical values as the experimental data (depending on time except for the latter).

Experimental Data Use

The choice of used experimental data is important as it defines which panel in the room will be simulated. For the sake of accuracy, a panel situated near the water supply will be modelled. This choice has been done because there is more certainty on the water supply temperature for these panels. The following experimental data have then been used:

- The water supply temperature will be used in the model. The water flow rate will be used for computing the water-copper heat transfer coefficient.
- In order to compute the panel-ambient convection heat transfer coefficient, the surface temperature of panel 9 will be used. As can be seen in Section 4.3, panel 9 is one of the closest panel to water supply having a temperature sensor.
- The ambient temperature will be the measured operative temperature.

Finally, it shall be remembered that the used data come from single panels, this is not representative of all panels. Indeed, panel characteristics depend on the heat gains location and their position in the water loops.

8 Results and Model Validation

From the model described in Section 7. Different results can be extracted to compare them with experimental measurements. For the model validation, two of them will be considered:

- The panel central surface temperature. This variable will be extracted from the model and will be compared with the surface temperature of panel 9. This value is also used as model input as mentioned in previous section (the choice of this panel has the same justification as the one for experimental data use in previous section).
- The panel heat flux (heat extracted from the room). This variable is constituted of 2 heat fluxes from the model: the radiative and the convective heat fluxes between the panel and the ambient. These will be extracted from the model and summed. The result will be compared with the heat flux of panel 1 (the choice of this panel has a similar justification to the one of panel 9: this panel is the closest to the water supply instrumented with a heat flux sensor). However, as the heat flux sensors cover a large portion of the panels and other inaccuracies described in the work of Bogatu et. al. [24], it was chosen to also compare the model results with heat flux values computed as follows (same formula for the convection heat transfer coefficient as the model input):

$$HF = (h_c + h_r) \times (T_s - T_{op}) \quad (7)$$

Where the convection heat transfer coefficient h_c is computed as in Equation 6 and the radiation heat transfer coefficient h_r is equal to $5.5 \text{ W}/(\text{m}^2 \times \text{K})$ (a common hypothesis for radiant ceiling cooling [46]). T_{op} and T_s are respectively the operative and the panel surface temperature that have been measured during the experiments.

Using measurements coming from different panels could have an impact on results quality as the heat fluxes with coefficients computed with panel 9 data are compared with the measurements of panel 1. The impact it could have is for example an inaccuracy on the panel surface temperature as the supply water temperature is slightly different for these panels. This inaccuracy will then propagate to the heat flux values. This phenomenon seems hard to avoid because of the sensor placement in the experimental setup (See Figure 6).

8.1 Non-Occupancy Simulation

Figure 41 shows evolution of panel central temperature and heat flux over the non-occupancy period.

From 18:00 to 23:00, the water is circulated, so the heat flux is high and the panel temperature decreases fast. When the night operative temperature setpoint condition is satisfied in the room, water is not circulated anymore. The panel being colder than the room, it absorbs the heat passively (i.e. less intensely than with water circulation). This absorption lead the temperature to rise.

On the one hand, Figure 41 shows a really good fit of the model temperature evolution compared to the experimental one. As the PT1000 sensors are very precise (see Section 4.4), the difference could come from assumptions on the heat transfer coefficients or the fact that the top of the panel is considered as an adiabatic surface.

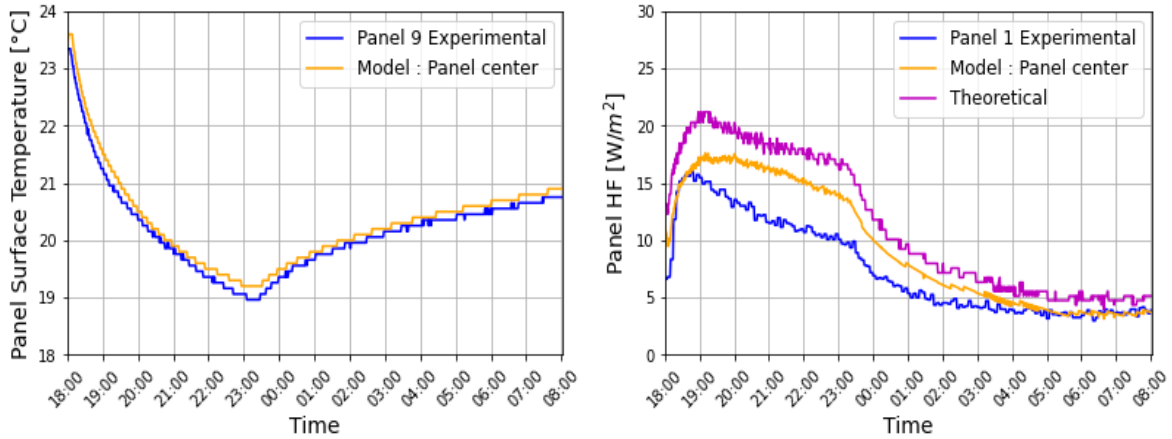


Figure 41: Model central panel surface data comparison with experimental data (non-occupancy).

On the other hand, the same figure shows that the model panel heat flux follows the same trend as both measurements and theoretical values. However, the error between the simulation and the other values is higher (indicators have been computed in Section 8.3). The same causes as above could explain this discrepancy. Finally, the assumption of the operative temperature as ambient temperature for convection and radiation could also induce some errors because panel 1 is situated in a corner of the room (See Figure 6). It is thus further from the operative temperature sensors and its radiation and convection heat transfers could also be influenced by this position.

8.2 Occupancy Simulation

Figure 42 shows that the heat transfer is overestimated by the model compared to the measurements. This could be a consequence of the same differences as mentioned in the previous sub-section. However, the model shows to follow the same trend as the theoretical values.

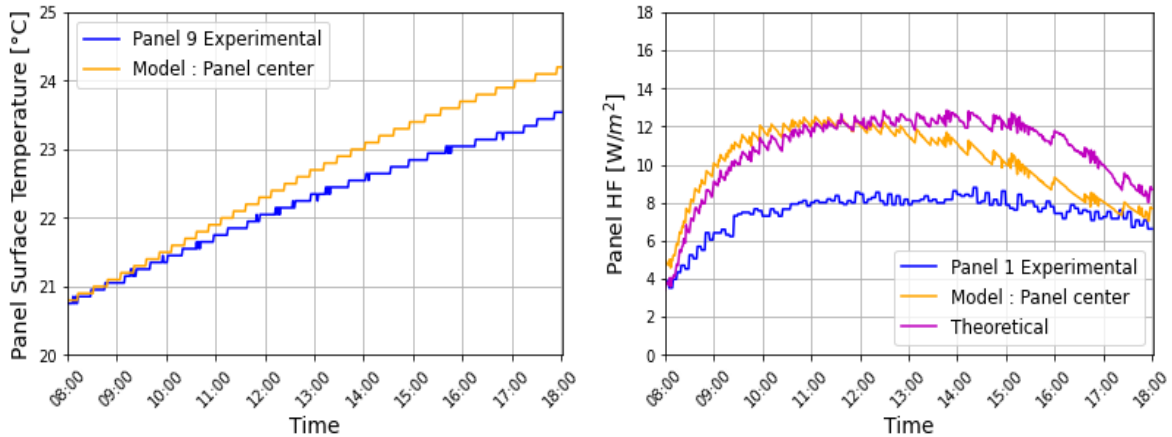


Figure 42: Model central panel surface data comparison with experimental data (occupancy).

During the occupancy, no water is circulated in the panel, causing it to heat up over time. The heat flux first increases sharply because of the introduction of heat gains at 8:00 (people arriving in the office). As a consequence, the room heats up rapidly and the panel temperature rises too, getting closer to the ambient temperature. This explains the descending trend of the heat flux at the end of the day. Finally, one can notice a maximum in the heat flux value close to noon. This parabolic trend can also be partly caused by the solar heat gains that manifest over time in the form of a parabola too.

As a consequence, the model temperature rises at a higher rate than the measured one. This leads both curve to diverge when the heat transfer values shows a big difference. In the end, the right behaviour is still shown by the model but the results show reduced precision.

8.3 Model Validation

According to Gallardo et. al. [47], a radiant ceiling panel with thermal energy storage model can be validated using a criteria based on root mean square error (RMSE) values. If the value of the RMSEs of the panel temperature and of the system power are respectively below 1.5 °C and 0.06 kW, the model is considered validated.

The following indicators were computed to compare the experimental values and the simulation:

$$RMSE_T = \sqrt{\sum_{i=1}^n \frac{(\hat{T}_i - T_i)^2}{n}} \quad \text{and} \quad RMSE_{\dot{Q}} = A_{ceil} \times \sqrt{\sum_{i=1}^n \frac{(\hat{HF}_i - HF_i)^2}{n}} \quad (8)$$

Where \hat{T}_i and \hat{HF}_i are respectively the model outputs corresponding to the measurements of T_i and HF_i (being the panel central surface temperature and the heat flux values) at the time step i for a data set of n values. In order not to compare a heat flux with a power, the RMSE of the heat flux will be multiplied by the sum of the area of all panels (as mentioned in Section 4.3, $A_{ceil} \approx 17 m^2$).

An indicator expressing the error of the model heat flux values with respect to the computed theoretical values of Equation 7 has also been computed in a similar way as $RMSE_{\dot{Q}}$ (this indicator is named $RMSE_{\dot{Q},Th}$).

The value of these indicators for both cases are listed in Table 14:

Table 14: Indicators for validation of the model for the two simulated time periods.

Model	RMSE _T	RMSE _{Q̇}	RMSE _{Q̇,Th}
Non-Occupancy (6pm to 8am)	0.17 [°C]	0.042 [kW]	0.036 [kW]
Occupancy (8am to 6pm)	0.43 [°C]	0.051 [kW]	0.024 [kW]

From these value, the model can be validated according to the source mentioned above. The heat flux errors with respect to the theoretical values are even smaller. This was expected as the model result curves were closer to the theoretical curves in Figures 41 and 42.

8.4 Study on Water Heat Extraction

As the model was validated, some interesting results can be extracted from the model. These interesting results are the heat extracted during water circulation (see Figure 34 for better representation of the parts of the model concerned):

- from the air to the copper tube,
- from the aluminium fin to the copper tube.

This has been done because no sensor can be placed to measure these values with introducing a perturbation in the system.

The mean conductive heat fluxes through the copper pipe from the model were extracted for each contact region describe in the bullet points above with respect to time. They were then multiplied by the contact length in order to yield values per panel length (the model being 2D). The results can be found in Figure 43:

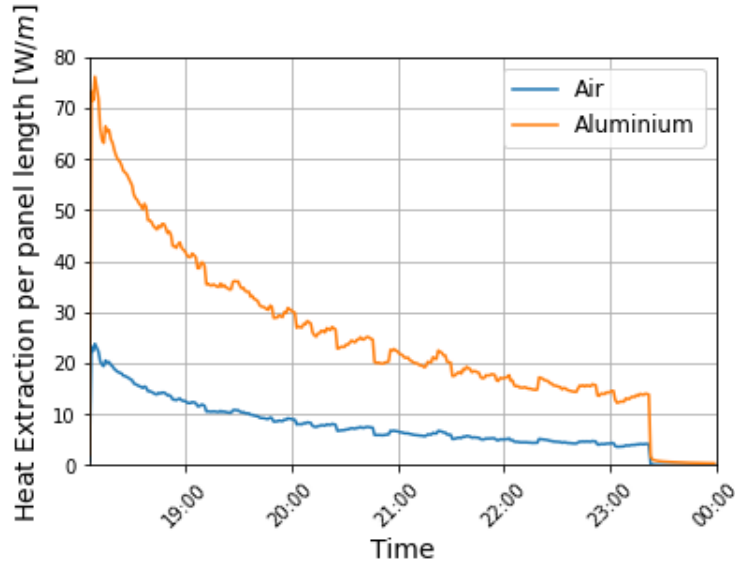


Figure 43: Heat extracted through the copper tube from the air layer and the aluminium fin.

The first 6 minutes were neglected because of their unstable results. The instability is due to the discontinuous initial conditions of the simulation.

By integrating these curves, it can be concluded that 148.1 Wh/m were extracted from the aluminium fin and 44.3 Wh/m were extracted from the air. The heat extraction from the air thus accounts for 23% of the total heat extraction and the one from the aluminium accounts for 77% of it (192.38 Wh/m were extracted in total).

9 Alternative Model : Simpler Model

As said in Section 6.2, one of the advantages of FEM is its ability to have results that could not be obtained through experiments because of the perturbation a sensor would represent to the system. It also takes the geometry of the technology into consideration.

With these statements in mind. A more simple model was elaborated. This model had many goals:

- Simulate with Finite Element Method a simpler model that could be implemented with other tools than finite elements which would lead a more precise solution.
- Compare this simpler model to experiments (to see if it can be validated too) and to the already validated model (for example to investigate a potential difference in PCM behaviour).
- Analyse this comparison to draw conclusions on a change of the panel geometry.

9.1 Definition of the Model

The newer model geometry, materials and stratification nomenclature of PCM sub-layers are represented in Figure 44 (the sub-layer nomenclature is similar for the first model during the comparison in Section 9.5):

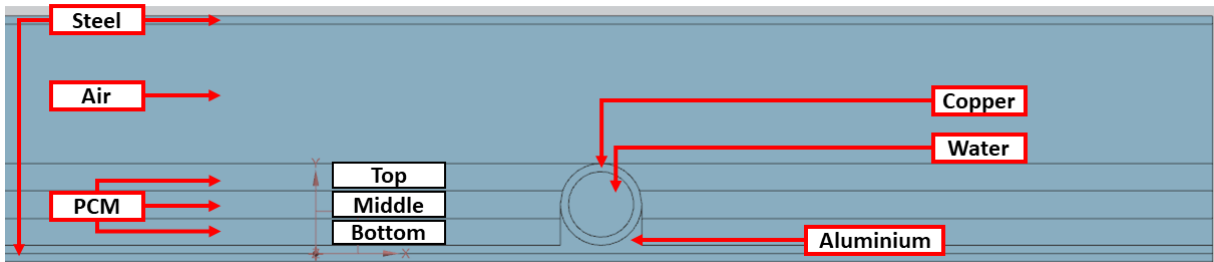


Figure 44: Geometry, materials and stratification nomenclature of PCM sub-layers of the simpler model.

One can see three main differences from previous model:

- The PCM has been sub-divided in 3 zones of same height. This will enable to represent the stratification of temperature in the panel and its evolution. Same division of the PCM will be done in the first mesh in order to be able to compare the results.
- The ferrite magnet has been removed for model simplicity. Also, this magnet is mainly used for mounting reasons in practice.
- The aluminium fin has been modified in order to have a simpler geometry. This change is expected to have the most influence on the panel results.

The newer model shares the same material properties as the old one. Also, as its geometry is quite similar, the same smallest element size will be used : 0.5 mm and will be applied in the same regions. Finally, the same simulations scenario as previous model (see Section 7.4) are conducted for this model so the results can be compared.

9.2 Model Simulation

Now that the model has been briefly defined, this section aims to show and provide comments about the model results to determine if it can be validated.

Non-Occupancy Simulation

In Figure 45, one can see that the model temperature evolution is very close to the measured one. One can also deduce that the temperature decreases faster for the simpler model than for the previous one. This can be explained by the change of the aluminium structure that now covers the entire steel plate. As aluminium has a greater thermal conductivity than steel, the heat extracted by the center of the panel can bypass the steel and causes a higher total heat removal in the steel through the aluminium. The absence of fin could also be an explanation. The fins used to enable the heat to by-pass the low thermal conductivity of the PCM. Now that these have been removed, less heat can go in the PCM. This leads the temperatures to drop faster in that area (also leading to higher heat fluxes).

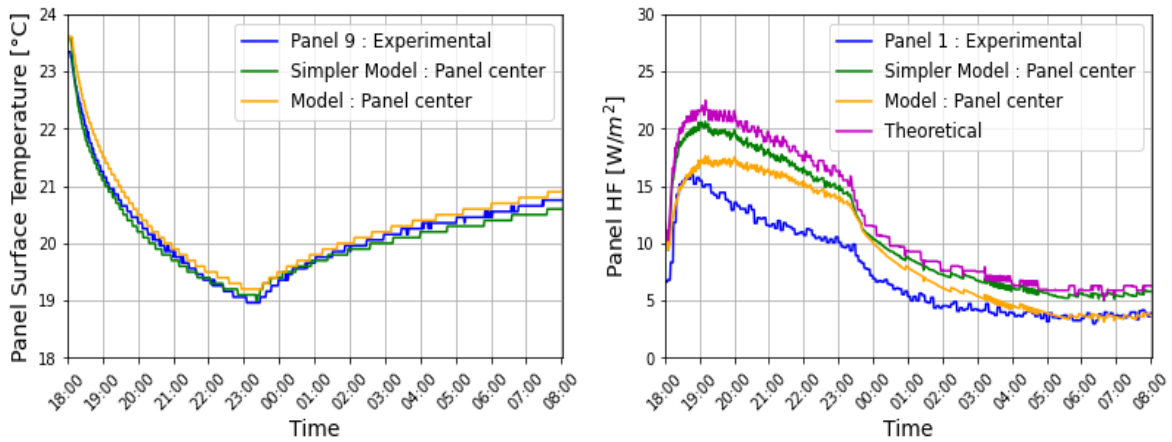


Figure 45: Simpler model comparison with experimental data and first model (non-occupancy).

However, a bit stranger behaviour occurs after the water circulation (after more or less 23:30). What could be expected is that the heat flux would be lower because of the removal of the fins but the panel surface temperature is smaller when there are no fins. This could be due that the fact that the variables of the model are considered in the panel center. It shall be remembered that the panel center corresponds to either the bottom left or the bottom right corner of the model. As can be seen in Figure 44, this location has now a better thermal connection with the center thanks to the extension of the aluminium plate. This improves the thermal connection with the rest of the panel whereas the first model concentrates the thermal connection more in the center of the panel, leading to that local difference in heat removal.

Apart from these observations, Figure 45 shows that the model heat flux curve follows the theoretical heat flux curve very closely.

Occupancy Simulation

Figure 46 highlights the same differences between the two models as for the non-occupancy case when the water circulation stops.

Once again, the simpler model temperature increases at a slower rate. This induces a higher value of the heat flux. This can be explained again by the shape of the aluminium profile and the fact that it provides a bigger thermal connection in that location. The theoretical and the model curves evolve again with a very similar trend.

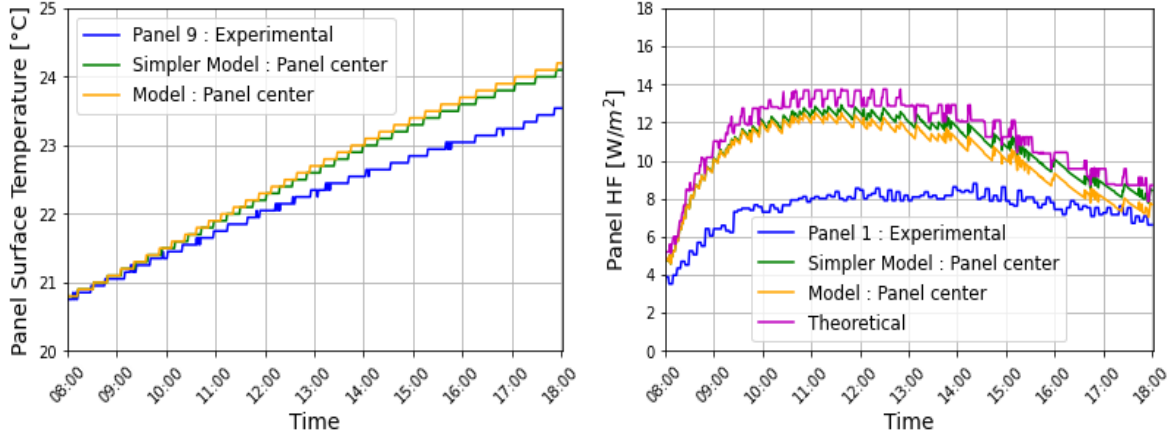


Figure 46: Simpler model comparison with experimental data and first model (occupancy).

9.3 Validation

Same criteria as in Section 8.3 will be used for trying to validate this model. In order to do so, the same indicators will be computed. The value of these indicators will also be compared with the ones of Section 8.3 in Table 15:

Table 15: Indicators for validation of the simpler model.

Model	$ \text{RMSE}_T $	$\text{RMSE}_{\dot{Q}}$	$\text{RMSE}_{\dot{Q},th}$
Non-occupancy	0.17 [°C]	0.042 [kW]	0.036 [kW]
Occupancy	0.43 [°C]	0.051 [kW]	0.024 [kW]
Non-occupancy (Simpler)	0.13 [°C]	0.064 [kW]	0.017 [kW]
Occupancy (Simpler)	0.36 [°C]	0.058 [kW]	0.013 [kW]

The night-time model presents too high flow rate values to be validated. This high values might come from the change in the aluminium profile that could enhance the heat flux in that zone. Also, the same remarks as in Section 8.3 concerning the results could explain the high RMSE values (i.e. temperature measurements from panel 9 are used to compute heat flux results that are compared with panel 1 measurements, panel 9 and panel 1 do not exactly have the same water supply temperature. This leads to a slight difference in other variables).

Note that the temperature indicators are more than $1\text{ }^{\circ}\text{C}$ lower than the maximum accepted value and the heat flux indicators are very close to the maximum accepted value. Also, the values of $|\text{RMSE}_{\dot{Q}_{\text{th}}}|$ are very low, this shows that the model seems accurate from a theoretical point of view.

9.4 Study on Water Heat Extraction

Before studying the PCM temperature stratification of the model, the same type of study on heat extraction than for last model can be conducted. From Figure 44, it is possible to distinguish two contacts of interest:

- between the copper tube and the aluminium fin,
- between the copper tube and the PCM.

The mean conductive heat fluxes through these contacts were extracted for each contact with respect to time. These were again multiplied by the contact length in order to yield values per panel length (the model being 2D). The results can be found in Figure 47:

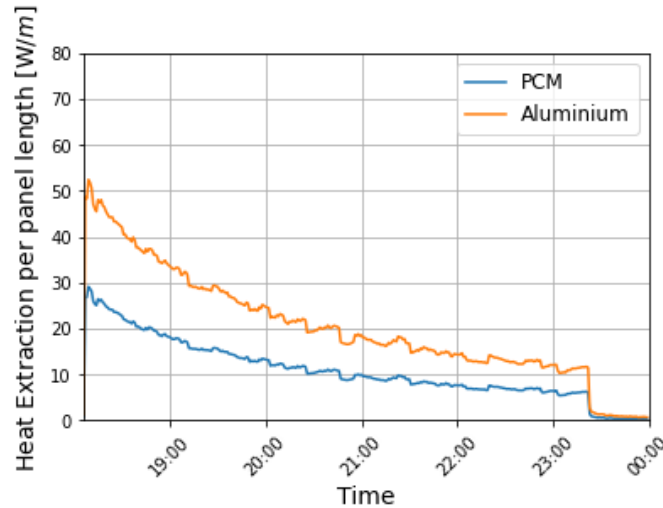


Figure 47: Heat extracted through the copper tube from the air layer and the aluminium fin (simple model).

The first 6 minutes were again neglected because of their unstable results. The instability is due to the discontinuous initial conditions of the simulation.

By integrating these curves, it can be concluded that $119.3\text{ }Wh$ were extracted from the aluminium fin and $64.1\text{ }Wh$ were extracted from the PCM. The heat extraction from the PCM thus accounts for 35% of the total heat extraction and the one from the aluminium accounts for 65% of it.

By comparing with Figure 43, less heat was extracted by this model compared to the previous one ($183.4\text{ }Wh/m$ for the simpler model compared to $192.4\text{ }Wh/m$ for the first one). This is because less heat is extracted from the aluminium. This could be explained by the absence of the fins in the simpler model. Also, the PCM has a better conductivity than air, thus it occupies a bigger share of the total heat extraction.

9.5 PCM Temperature Stratification Comparison

As said in Section 6.2, one of the advantages of Finite Element Method is that it can provide results that could not be measured experimentally. This enables to compare the difference of behaviour in PCM temperature inside the panel. This will give insights of the real impact of the aluminium fin. For the two models presented before, the PCM layer was divided in parts of the same height (3.33 mm each) and the mean of the PCM temperature in each layer has been computed for every time step.

Non-Occupancy Simulation

This part will focus on the non-occupancy simulation (from 18:00 to about 8:00). The results for this time interval are shown in Figure 48.

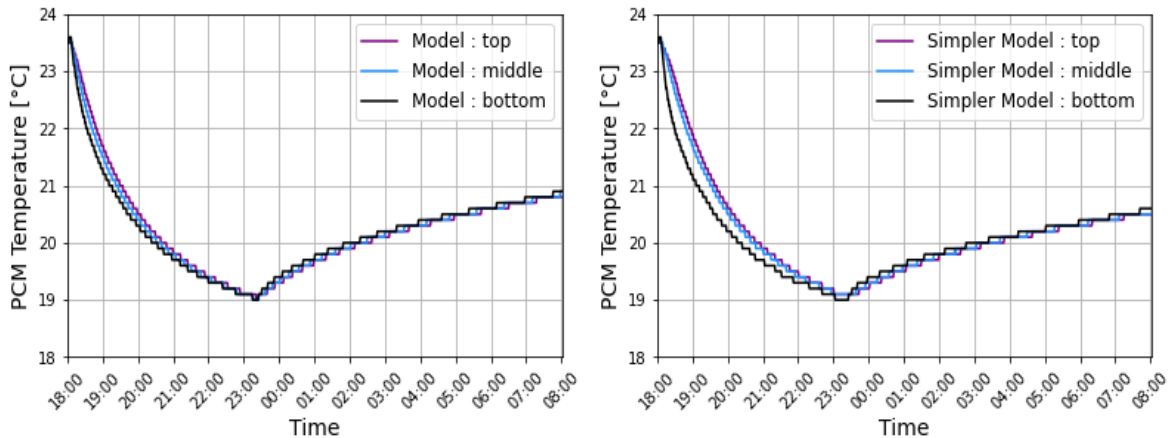


Figure 48: Comparison of the PCM temperature stratifications of the 2 models (non-occupancy).

The first noticeable information is in the global temperature evolution of the two models: The two models have a very similar global temperature evolution, reaching about $19^{\circ}C$ as minimum temperature. This is because the models have been simulated with the same boundary conditions. This means that the main difference will be in the temperature stratification.

A second, more subtle observation is that the bottom layer temperature of the simpler model is evolving differently than the two other layer's temperatures. It can be explained by the low thermal conductivity of the PCM and the absence of a vertical conductive bridge. On the opposite, the other model has this conductive bridge and thus more uniformity in the different layer temperatures.

In addition, by comparing the two models for every layer, small differences start to be evident. In Figure 49, it can be observed that the top and middle temperatures of the simpler model lag the predictions of the first model (i.e. the bottom curve value at a certain time is often achieved later by the other curves). The opposite can be stated for the bottom layer. This shows that the aluminium fins enhance the conductivity between the PCM layers when water is circulating.

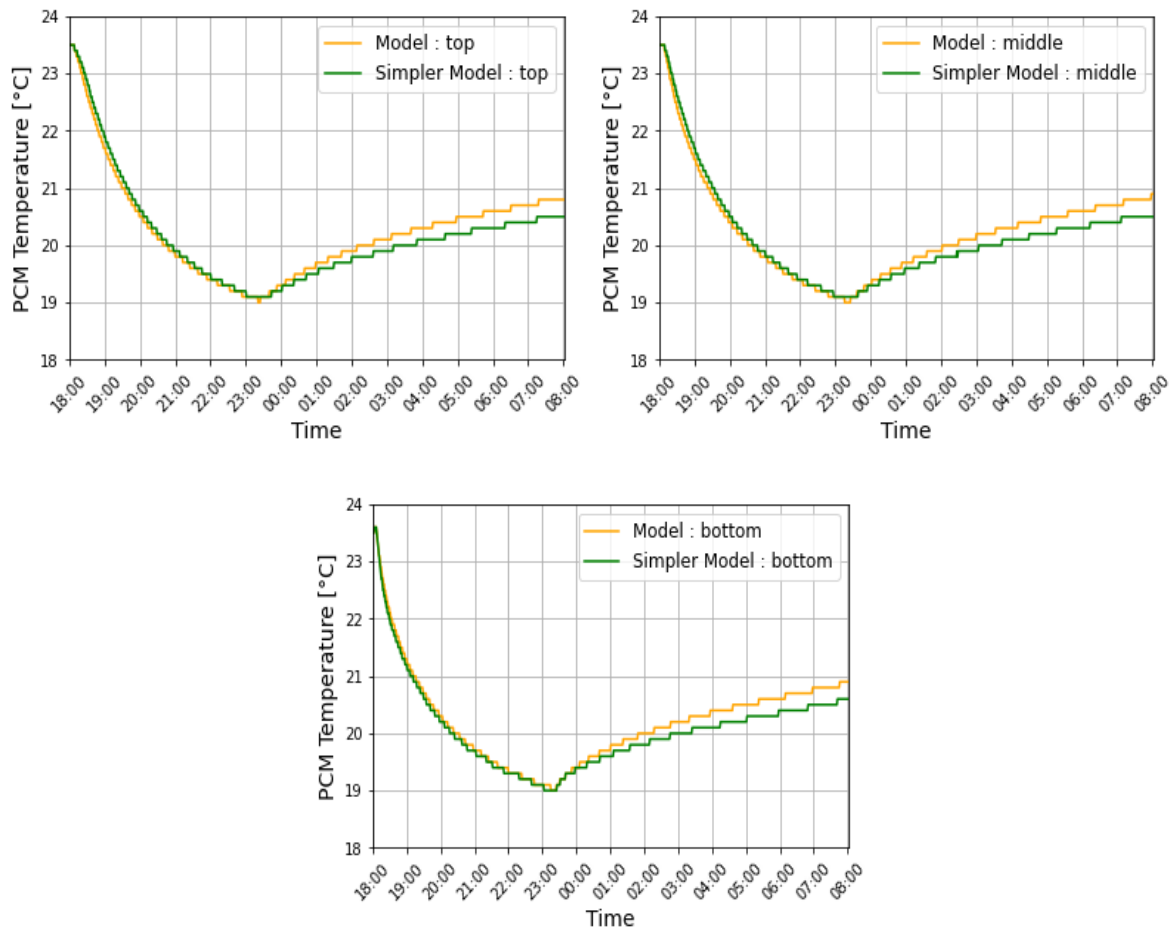


Figure 49: Comparison of the PCM temperature stratifications of the 2 models per layer (non-occupancy).

Focusing now on the rest of the interval (from about 23:30 to 8:00). One can see in Figure 48 that the PCM temperatures evolve quite uniformly for the two models. However, the difference is on the global trend. The temperatures of the first model are significantly higher than the ones of the simpler model. These results are coherent with the results of Section 9.2.

Occupancy Simulation

Figure 50 shows the results for the occupancy simulation (from 8:00 to 18:00). Here the results and the conclusions are similar to the ones of the non-occupancy simulation when the water is not circulating (from about 23:30 to 8:00). In fact, the layer temperatures evolve in a uniform way for the two models but they reach lower values for the simpler one. Same analysis and conclusions as Section 9.2 can be drawn.

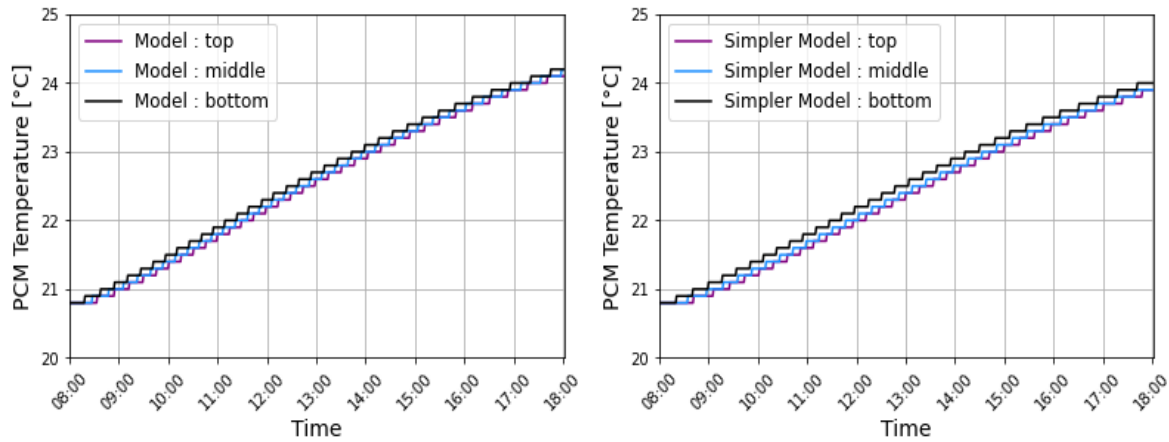


Figure 50: Comparison of the PCM temperature stratifications of the 2 models (occupancy).

9.6 Discussion

To sum up, a simpler model has been designed in order to investigate the impact of the geometry of the aluminium structure and to try to give more credit to models with less geometrical precision than Finite Element ones.

According to the validation criteria used for the previous model (see Section 8.3), this simpler model well represents the charging behaviour of the PCM panel. However, it lacks a bit of precision with its heat flux results during its discharging behaviour (non-occupancy). This non-validation can be explained by the different geometry of this model compared to the real panel itself. Also, changing and/or refining some assumptions could help the validation of this model. This could be matter of further investigation. However, if the heat flux were to be compared with computed theoretical values, then the model presented very small RMSE values and could be validated.

Nevertheless, this model pointed out interesting results concerning the internal behaviour of the PCM. For example, it showed the effect of the vertical fins on the PCM temperature stratification as a thermal conductivity enhancer. Another interesting result is that the model extracted less heat through the water circulation pipe than the first model (this could due to the absence of vertical fin).

10 Other Geometry : Model Derived From TABS

As said in Section 6.2, Finite Element Method allows to simulate model with good precision by taking into account the model geometry. These advantages can allow to design and compare models with very different geometries.

In this section, a new model has been designed to verify the error introduced by panel geometry and material property alterations. These are required due to flexibility limitations of models available in building performance simulation softwares. For example, Yasin et. al. [48] aimed to create an equivalent model of PCM panel. This equivalent model is based on a TABS (Thermally Activated Building Systems) model and was elaborated because the TRNSYS software does not have a pre-built model for PCM panels. One thing that is often done is to design a TABS model and adjust its parameters in order to fit the panel's results. As FEM allows to give precise results and to take geometry into account, a model has been created to verify the impact on results of the geometry change and of some assumptions similar to the ones in the previously mentioned study.

10.1 Geometry, Assumptions and Materials Definition

The geometry of the panel model has been changed in order to satisfy the geometry requirements of the type 399 TRNSYS model (shown in Figure 51).

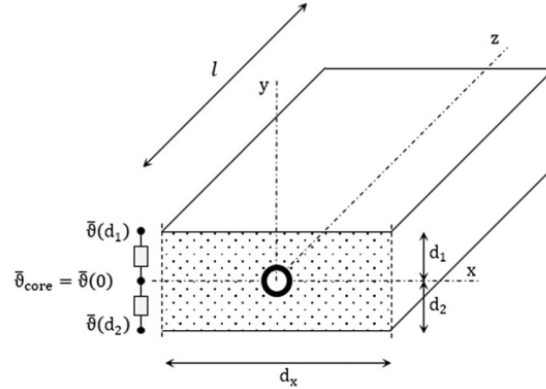


Figure 51: Geometry of the TABS model as modelled in TRNSYS [48].

For the TABS model to work, the model has to satisfy geometrical constraints:

$$\frac{d_1}{d_x} > 0.3 \quad \text{and} \quad \frac{\delta}{d_x} < 0.2 \quad (9)$$

Where (values in parentheses are the values for the simpler model's geometry):

- d_1 is the length between the higher boundary of the model and the center of the fluid circulation pipe (5 mm).
- d_x is the width of the model (150 mm).
- δ is the fluid circulation pipe outer diameter (10 mm).

The parameter that will be varied is thus d_1 . It will be set to 45 mm in order to bound Equation 9. Other constraints are that the pipe shall be in the middle of the storage material and that the pipe shall transmit heat (virtually) in an even way on all the width of the model (as if the horizontal x axis was a perfectly conductive material).

In order to satisfy these constraints while having a similar geometry to the simpler model, a new model was created. It is represented in Figure 52.

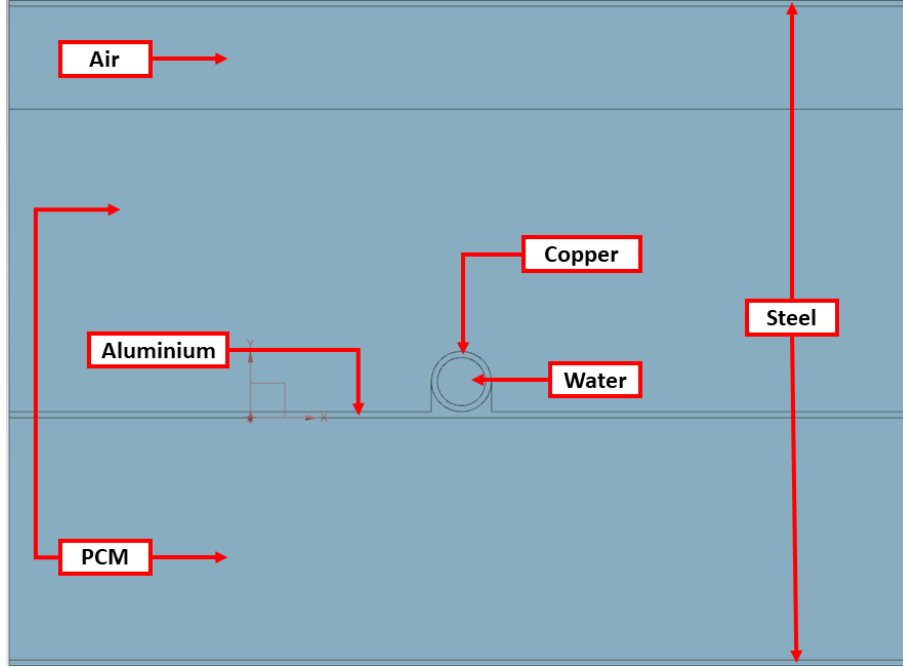


Figure 52: 2D TABS equivalent model geometry with materials description.

The different materials will have similar properties than the ones of the two models (see Section 7.1) except for the PCM. One of the assumptions made in the paper is that a correcting factor can be used to adjust the thermal conductivity and the density of the PCM to get a similar behaviour to the previous models. This correcting factor will be the ratio of the areas of the PCM part in the TABS equivalent and simpler models. The definition and the application of this factor can be seen in Equations 10 and 11.

$$k = \frac{A_{PCM,TABS}}{A_{PCM,simpler}} \approx 11.5 \quad (10)$$

$$\lambda_{PCM,TABS} = k \times \lambda_{PCM,simpler}, \rho_{PCM,TABS} = \frac{\rho_{PCM,simpler}}{k} \quad (11)$$

The thermal conductivity of the PCM ($\lambda_{PCM,TABS}$) and its density ($\rho_{PCM,TABS}$) are now respectively of $2.3 \frac{W}{m \times K}$ and $71.74 \frac{kg}{m^3}$. The other PCM properties remain unchanged and are equal to the ones in Section 4.1. One of the purpose of the model is to verify the effects of this assumption on the results.

The assumptions of Section 7.2 will still be used for this model.

10.2 Choice of Meshing Size and Simulation

As the geometry of the model changes drastically in last section, a new mesh was designed. As the model's size is much greater than the one of the previous model, a bigger element characteristic size has been used for the PCM (2 mm) in order to keep similar computation times. The parts where more precision could be needed kept the 0.5 mm size defined in Section 7.3. These parts are the steel and aluminium plates, the copper tube and the water. These changes yield the mesh in Figure 53:

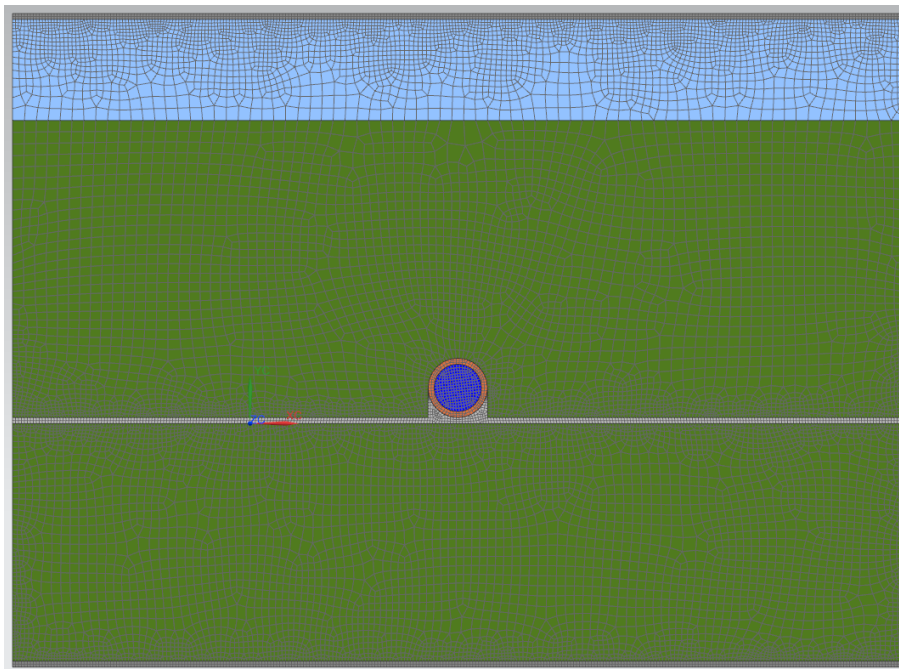


Figure 53: 2D TABS equivalent model mesh.

The simulation boundary conditions remain unchanged with respect to the two previous models (see Section 7.4).

10.3 Results and Validation

The simulations have been run for the two scenarios. The results are compared with the experimental ones to attempt a model validation. Moreover, the results of the simpler model are used for comparison too in order to see the impact of the change of geometry itself. Once again, the results displayed are the ones in the considered center of the panel.

Non-Occupancy Simulation

As can be seen in Figure 54, the TABS equivalent model shows results having a good trend for temperature and a similar one to the simpler model for the heat flux. The TABS model heat flux curve is also very close to the theoretical model heat flux curve.

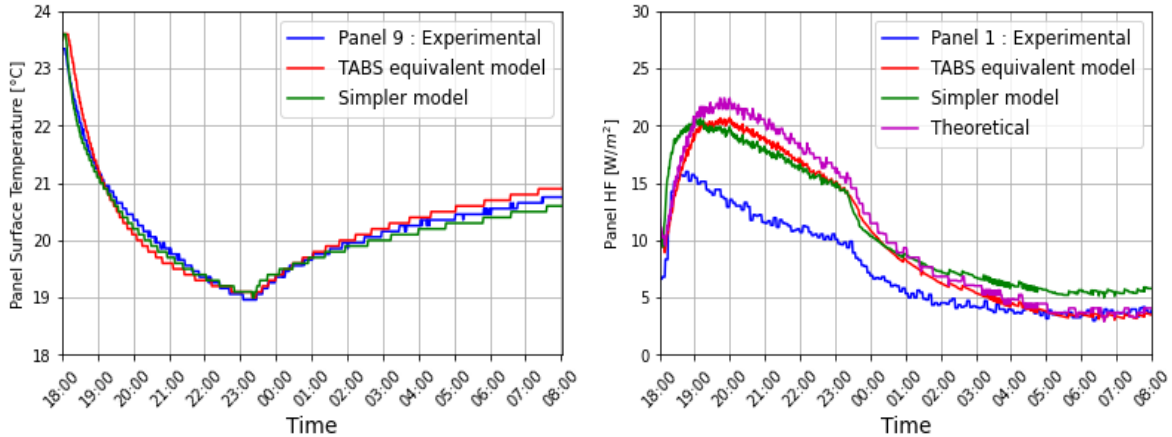


Figure 54: TABS equivalent model comparison with experimental data and simpler model (non-occupancy).

Something noticeable is that there is a heat flux delay at the beginning of the simulation. This happens during the water circulation phase (from 18:00 to 23:30). It can be caused by the bottom PCM layer that acts as a buffer for the heat flux. As there is no more direct contact between the aluminium plate and the steel plate (especially in the center of the panel), the heat absorbed by the circulating water cannot bypass the PCM layer.

However, after the lagging period the results come very close to the simpler model. This shows that the assumption on the storage material density and conductivity is able to mimic the right behaviour. When the water stop circulating (after 23:30), the results converge even closer to the experimental ones. One explanation is that the steel plate is not in contact with the aluminium plate anymore, leading to a behaviour closer to the first model.

Occupancy Simulation

Figure 55 shows that the simpler and the TABS equivalent models have similar behaviour in charging mode (during the day).

The temperatures evolve in a similar way except that the TABS equivalent model temperatures evolve faster. This might be due to the PCM layer that isolates the steel layer from the rest of the structure. In the simpler model, the steel plate was linked to the aluminium structure that increased the contact area with the PCM, allowing more heat flux to go through. This causes the temperatures of the steel plate to evolve slower. This could also explain the higher heat flux during the day (from 8:00 to 18:00) and during the night when the water stops circulating (from 23:30 to 8:00).

Finally, the TABS model results are again very close to the theoretical ones in terms of heat flux.

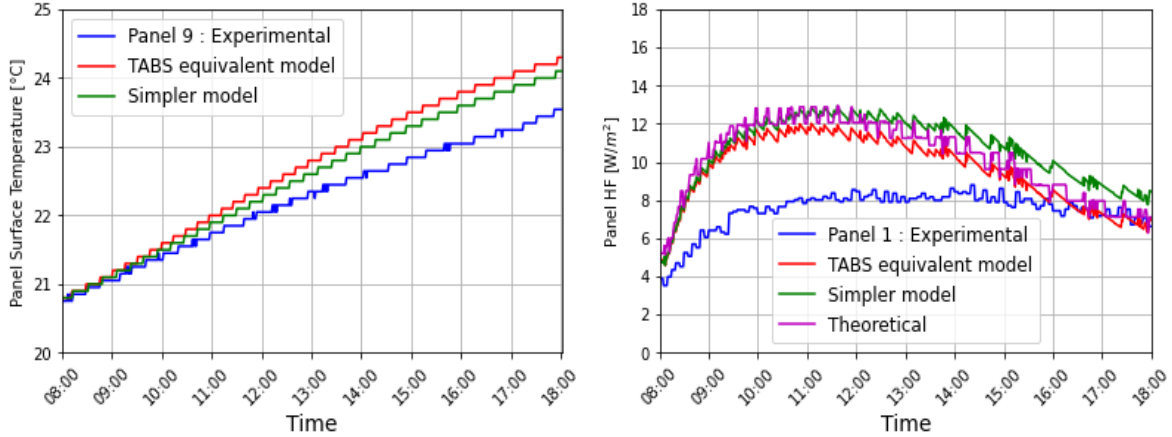


Figure 55: TABS equivalent model comparison with experimental data and simpler model (day).

Model Validation

Once again, same criteria as in Section 8.3 will be used for trying to validate this model (implying the computation of the same indicators). The value of these indicators was compared with the ones of the two last models from Section 8.3 and 9.3 in Table 16:

Table 16: Indicators for validation of all 3 models.

Model	$ \text{RMSE}_T $	$\text{RMSE}_{\dot{Q}}$	$\text{RMSE}_{\dot{Q},Th}$
Non-occupancy	0.17 [$^{\circ}C$]	0.042 [kW]	0.036 [kW]
Occupancy	0.43 [$^{\circ}C$]	0.051 [kW]	0.024 [kW]
Non-occupancy (Simpler)	0.13 [$^{\circ}C$]	0.064 [kW]	0.017 [kW]
Occupancy (Simpler)	0.36 [$^{\circ}C$]	0.058 [kW]	0.013 [kW]
Non-occupancy (TABS equivalent)	0.17 [$^{\circ}C$]	0.063 [kW]	0.035 [kW]
Occupancy (TABS equivalent)	0.51 [$^{\circ}C$]	0.043 [kW]	0.031 [kW]

From the table, the first conclusion is that the model cannot be validated according to the criteria with respect to the measurements. As a matter of fact, the indicator of the system power for the non-occupancy simulation is again slightly too high (as a reminder, it shall be smaller than 0.06 kW). The temperature results are however almost both $1^{\circ}C$ below the required value for validation. The TABS equivalent model can be compared with the simpler model its derived from. The latter has a better representation of the panel temperature whereas the former represents better the heat fluxes.

However, the model can be validated with respect to the theoretical results from Equation 7. Indeed, the heat flux indicators are more than 20 W under the maximum acceptable value.

In the end, both models have similar level of accuracy in representing PCM panels with respect to measurements. This is the results that had to be verified. As for the simpler model, this model could be validated with better assumptions. However, with respect to the theoretical results, all three models can be validated and it is even noticeable by looking the indicators in Table 16 that the simpler model is more precise than the first model which is itself more precise than the TABS equivalent model.

11 Discussion

This simulation investigation using Finite Element Method had many goals. Such as creating and attempting to validate several 2D models. One had the same geometry as a real panel, the second one had a simpler geometry and the last one was designed to be similar to a TRNSYS Type 399 TABS model with altered PCM properties.

In conclusion, the first model was validated using a criteria in the work of Gallardo et. al. [47]. This validation used the simulation results at the center of the panel to match sensor location. This model became the baseline for the further studies. In addition, a study on heat extraction by the water circulation was performed. The main conclusion is that 77% of the heat the water extracted went through the contact between the copper pipe and the aluminum structure and the remaining 23% came from the air.

The second model was designed with a simplified aluminium structure. It yield good results but failed to be completely validated with respect to measurements. The fact that the aluminium fin covered the steel plate entirely had a significant local impact on the region where the results were sampled. This happened especially when water circulation was active. However, the model had the best indicators when compared with theoretical results using measurements. Moreover, a study on heat extraction by the water circulation was performed again. The main conclusion is that 65% of the heat the water extracted went through the contact between the copper pipe and the aluminum structure and the remaining 35% came directly from the PCM. Finally, a study on the PCM temperature stratification was conducted for the two model (realistic and simpler). The main conclusion of this investigation is that the aluminium fin lightly enhanced the thermal conductivity inside the phase change material, especially in charging mode (during occupancy).

Finally, a TABS equivalent model has been created by changing the geometry and by modifying the PCM parameters. It yield similar results to the simpler model. It thus failed to be validated with measurements but showed that there is a certain degree of equivalence between the models. It also succeeded to be validated using Equation 7 that used measurements.

12 Conclusion

In the course of this thesis an experimental study was performed. It showed that without ventilation, day-water circulation was required when the system faced a high heat load (6 occupants with computers). It also showed that a correct choice of parameters related to water circulation (temperature setpoints for activation) and ventilation (inlet temperature and flowrate) allowed to achieve an excellent level of thermal comfort (95.8% of the time in Category II including 92.1% of the time in Category I). In that context, the panels were behaving like radiant panels. These results came with the cost of intense water circulation during the day. Future work could be to fine tune these parameters in order to achieve similar thermal comfort by reducing the intensity of the water circulation. In opposite, a bad choice of these parameters could decrease thermal comfort when ventilation is added (compared to a case in which panels would operate on their own). In that context, the MEPs were behaving like TABS. These results highlighted that the setpoints related to ventilation and water circulation determined whether the system behaved like radiant panels or like TABS. Finally, results showed that day-active water circulation allowed to improve panel heat flux of 35% (from 15.4 W/m^2 to about 21 W/m^2).

A simulation oriented investigation using Finite Element Method was also conducted. In the course of that investigation, three models were designed. The first a was realistic model designed using measurements of a panel profile. It succeeded to be validated using both temperature (RMSE of 0.17°C during occupancy and RMSE of 0.43°C during non-occupancy) and heat rate measurements (RMSE of 0.042 kW during occupancy and RMSE of 0.051 kW during non-occupancy). A study on heat extraction showed that 77% of heat extracted during water circulation came from the aluminum profile and 23% came from the air layer. A second model was then designed using a simpler aluminum profile that failed to be validated because with respect to heat flux measurements. It however showed better results with respect to temperature measurements (RMSE of 0.13°C during occupancy and RMSE of 0.36°C during non-occupancy) and with respect to a theoretical correlation for heat rate using experimental measurements (RMSE of 0.017 kW during occupancy and RMSE of 0.013 kW during non-occupancy). A study on heat extraction showed that 65% of heat extracted during water circulation came from the aluminum profile and 35% came from the PCM layer. It was compared to the first model in terms of PCM temperature stratification. The main conclusion drawn from this comparison was that the aluminum fins indeed improved thermal conductivity in the PCM layer, especially during occupancy. Finally, a third model has been designed with a similar geometry as the TRNSYS Type399 TABS model. Alterations of the PCM characteristics were assumed to allow to reproduce the behaviour of a MEP using that geometry. In the end, the model could be validated using temperature measurements (RMSE of 0.17°C during occupancy and RMSE of 0.51°C during non-occupancy) and the theoretical correlation for heat rate using experimental measurements (RMSE of 0.035 kW during occupancy and RMSE of 0.031 kW during non-occupancy).

References

- [1] *2030 climate & energy framework* - **European Commission** : https://climate.ec.europa.eu/eu-action/climate-strategies-targets/2030-climate-energy-framework_en (08/06/2023)
- [2] *2050 long-term strategy* - **European Commission** : https://climate.ec.europa.eu/eu-action/climate-strategies-targets/2050-long-term-strategy_en#:~:text=The%20EU%20aims%20to%20be,AgreementEN%E2%80%A2%E2%80%A2%E2%80%A2. (08/06/2023)
- [3] *Buildings, A source of enormous untapped efficiency potential* - **International Energy Agency** : <https://www.iea.org/topics/buildings>
- [4] *The Future of Cooling* - **International Energy Agency** : <https://www.iea.org/reports/the-future-of-cooling> (08/06/2023)
- [5] *PARAFFIN WAX TO BE USED AS PHASE CHANGE MATERIAL FOR ENERGY STORAGE* - **RAHA Paraffin Co** : <https://paraffinwaxco.com/phase-change-materials/> (09/03/2023)
- [6] *Phase change materials for building applications: A state-of-the-art review* - **R. Baetens, B. P. Jelle, A. Gustavsen** : <https://www.sciencedirect.com/science/article/pii/S0378778810001180> (09/03/2023)
- [7] *An overview of thermal energy storage systems* - **G. Alva, Y. Lin, G. Fang** : https://www.sciencedirect.com/science/article/pii/S036054421732056X?casa_token=VSfmm06HZH8AAAAA:xwN2S1Tr4w-Q2kxIythIpZvPkhSzvC3qx1FKr7Mpv-rZA7raDvgYpI-8z6uiDqUxUdDe72zAVM (23/05/2023)
- [8] *Energetic investigation of solar assisted heat pump underfloor heating systems with and without phase change materials* - **M. T. Plytaria, C. Tzivanidis, E. Bellos, K. A. Antonopoulos** : <https://www.sciencedirect.com/science/article/pii/S0196890418308550> (23/05/2023)
- [9] *In-situ study of thermal comfort enhancement in a renovated building equipped with phase change material wallboard* - **F. Kuznik, J. Virgone, K. Johannes** : https://www.sciencedirect.com/science/article/pii/S0960148110005100?casa_token=smWE_kcq2LQAAAAA:AGOhdJmysdG9s8_eyV6modrYmMRK0gyc1xaKzWhpLZkCYB-PFIAZYEgAU7ddgGD1hfEpUDb4t8U (23/05/2023)
- [10] *Thermal conductivity enhancement of phase change materials for thermal energy storage: A review* - **L. Fan, J.M. Khodadadi** : https://www.sciencedirect.com/science/article/pii/S1364032110002595?casa_token=zGkci18SEE0AAAAA:cC3AW3Q1W_mu4AnQK8JZGMYZBCUYNXPL4xjvsqc_pUh8JJAB993U-iAyFKlerNv_-GRGwJz_PGs (13/03/2023)
- [11] *Nanoparticles effect on freezing of PCM utilizing finite element approach* - **Y. Feng a, Y. Qin** : <https://www.sciencedirect.com/science/article/pii/S016773222201707X> (13/03/2023)

- [12] *Economic comparison of TABS, PCM ceiling panels and all-air systems for cooling of-fices* - **L. B. Boccardo, O. B. Kazanci, J. Q. Allerhand, B. W. Olesen** : <https://www.sciencedirect.com/science/article/pii/S0378778819313969> (13/03/2023)
- [13] *Review on thermal energy storage with phase change materials and applications, vol. 13, no. 2. 2009.* - **A. Sharma, V. V. Tyagi, C. R. Chen, D. Buddhi** : <https://www.sciencedirect.com/science/article/pii/S1364032107001402> (19/04/2023)
- [14] *Impregnation of porous material with phase change material for thermal energy storage* - **T. Nomura, N. Okinaka, T. Akiyama** : https://www.sciencedirect.com/science/article/pii/S025405840900128X?casa_token=1S00EkFMZYIAAAAA:mQun-hO_CPMX1rIGBR7ZUwvRONLOR6nB6ydiNIPqiAopFtoSz6hCmd_SDgqfk6gNWVQWRh8FvDt (19/04/2023)
- [15] *Preparation, thermal performance and application of shape-stabilized PCM in energy efficient buildings* - **Y.P. Zhang, K.P. Lin, R. Yang, H.F. Di, Y. Jiang** : <https://www.sciencedirect.com/science/article/pii/S0378778806000776> (19/04/2023)
- [16] *Development of a thermally activated ceiling panel with PCM for application in lightweight and retrofitted buildings* - **M. Koschenz, B. Lehmann** : <https://www.sciencedirect.com/science/article/pii/S0378778804000702> (20/04/2023)
- [17] *A review on energy conservation in building applications with thermal storage by latent heat using phase change materials* - **A. M. Khudhair, M. M. Farid** : https://www.sciencedirect.com/science/article/pii/S0196890403001316?casa_token=y9qcGzzM10MAAAAA:qmczHp9dLnHvc63U458LrLemLb_PWU24Z6M73f0tj1i1LVq41B7YDPkVMH1MIntbRBse__HinbyS (20/04/2023)
- [18] *Energy performance of buildings - Ventilation for buildings - Part 1: Indoor environmental input parameters for design and assessment of energy performance of buildings addressing indoor air quality, thermal environment, lighting and acoustics - Module M1-6 - DANSK STANDARD/EN 16798-1:2019* : (30/05/2023)
- [19] *Ergonomics of the thermal environment - Analytical determination and interpretation of thermal comfort using calculation of the PMV and PPD indices and local thermal comfort criteria - DANSK STANDARD/ISO 7730* : (25/05/2023)
- [20] *PCM cooling ceilings in the Energy Efficiency Center—passive cooling potential of two different system designs* - **H. Weinläder, F. Klinker, M. Yasin** : <https://www.sciencedirect.com/science/article/pii/S0378778816301682?via%3Dihub> (24/05/2023)
- [21] *Analysis of the energy and thermal performance of a radiant cooling panel system with integrated phase change materials in very hot and humid conditions* - **A. Gallardo, U. Berardi** : <https://iopscience.iop.org/article/10.1088/1757-899X/609/5/052025> (24/05/2023)
- [22] *Thermal and energy performance evaluation of a full-scale test cabin equipped with PCM embedded radiant chilled ceiling* - **S. Mousavi, B. Rismanchi, S. Brey, L. Aye** : <https://iopscience.iop.org/article/10.1088/1757-899X/609/5/052025> (24/05/2023)
- [23] *Energy and thermal comfort performance evaluation of PCM ceiling panels for cooling a renovated office room* - **J. Q. Allerhand, O. B. Kazanci, B. W. Olesen** : <https://www.mdpi.com/2073-4360/12/4/818> (04/05/2023)

- [24] *An experimental study of the active cooling performance of a novel radiant ceiling panel containing phase change material (PCM)* - **D-I. Bogatu, O. B. Kazanci, B. W. Olesen** : <https://www.sciencedirect.com/science/article/pii/S0378778821002656> (04/05/2023)
- [25] *Performance characterization of a novel ceiling panel with Phase Change Materials (PCM), Master Thesis* - **A. H. S. Hansen**
- [26] *A Resiliency Approach to Radiant Ceiling Panels with Phase Change Materials, Master Thesis* - **J. FeBl** (04/05/2023)
- [27] *Energy and Indoor Environmental Quality Performance of Radiant Ceiling Panels with Phase Change Materials, Master Thesis* - **A.Sotirios** (04/05/2023)
- [28] *Economic comparison of TABS, PCM ceiling panels and all-air systems for cooling offices* - **L. B. Boccardo, O. B. Kazanci, J. Quesada Allerhand, B. W. Olesen** : <https://www.sciencedirect.com/science/article/pii/S0378778819313969> (04/05/2023)
- [29] *RT 24 Datasheet, Berlin: Rubitherm Technologies GmBh, 2018.* - **Rubitherm** : (18/04/2023)
- [30] *D6.3 Report on the usability of TABS panels (radiant ceiling panels with PCM)* - **DTU** (20/04/2023)
- [31] *New indoor environment chambers and field experiment offices for research on human comfort, health and productivity at moderate energy expenditure* - **J. Toftum, G. Langkilde, P.O. Fanger** : <https://www.sciencedirect.com/science/article/pii/S0378778804000970?via%3Dihub> (25/05/2023)
- [32] *ICIEE : DOCUMENTATION MANUAL RADIANT HEATING & COOLING SYSTEM CHAMBER 6 BUILDING 412* - **D-I. Bogatu** : (25/05/2023)
- [33] *Engineering Guide Displacement Ventilation* - **Price Industries** : <https://www.priceindustries.com/content/uploads/assets/literature/engineering-guides/displacement-ventilation-engineering-guide.pdf> (25/05/2023)
- [34] *Ergonomics of the thermal environment - Instruments for measuring physical quantities* - **Dansk Standard/ISO 7726** : (07/06/2023)
- [35] *PT1000 documentation* - **RS website** : <https://docs.rs-online.com/9186/0900766b815bb292.pdf> (26/05/2023)
- [36] *Kamstrup multical 602 documentation* - **Kamstrup Website** : <https://www.kamstrup.com/en-en/heat-solutions/meters-devices/discontinued-products/multical-602/documents> (26/05/2023)
- [37] *gSKIN-XI documentation* - **GreenTeg Website** : <https://shop.greenteg.com/heat-flux-sensor-gskin-xi/> (26/05/2023)
- [38] *SensoAnemo documentation* - **Manualslib** : <https://www.manualslib.com/manual/1310017/Sensor-Electronics-Airdistsys-5000.html#manual> (26/05/2023)
- [39] *Introduction to Finite Element Method (FEM) for Beginners* - **Solid Mechanics Classroom** : <https://www.youtube.com/watch?v=C6X9RyO2mPU>(03/05/2023)
- [40] *Application of the Finite Element Method in the Analysis of Composite Materials: A Review* - **S. D. Müzel, E. P. Bonhin, N. M. Guimarães, E. S. Guidi** : <https://www.mdpi.com/2073-4360/12/4/818> (03/05/2023)

- [41] *A parametric study on radiant floor heating system performance* - **S. Sattari, B. Farhanieh** : https://www.sciencedirect.com/science/article/pii/S0960148105002624?casa_token=WgIRtHhDwskAAAAA:DWF6yi0JVv-a9y7h12LcpJFAqVmJ04dH_uJgEhqEfo-3_2R1Bh0czp1M5RMZA25GsBuWQAlfBBiR (03/05/2023)
- [42] *Realization, test and modelling of honeycomb wallboards containing a Phase Change Material* - **C. Hasse, M. Grenet, A. Bontemps, R. Dendievel, H. Sallée** : https://www.sciencedirect.com/science/article/pii/S0378778810003373?casa_token=dcD1MXjwYgAAAAA:8usxjYPN4kkb1FG7S0gMwyGj_mknIfMhOmtGEgJ3tnXDHKx085Mnym49k24DZ881A_OF3cCxWdZ (03/05/2023)
- [43] *A simplified model for radiant heating and cooling panels* - **i.B. Kilkis, S.S. Sager, M. Uludag** : <https://www.sciencedirect.com/science/article/pii/S0928486994900140> (03/05/2023)
- [44] *Emissivity Coefficients common Products* - **Engineering Toolbox** : https://www.engineeringtoolbox.com/emissivity-coefficients-d_447.html (12/05/2023)
- [45] *Building environment design - Design, dimensioning, installation and control of embedded radiant heating and cooling systems - Part 2: Determination of the design heating and cooling capacity (ISO 11855-2:2012)* - **Dansk Standard** : (12/05/2023)
- [46] *A review of the surface heat transfer coefficients of radiant heating and cooling systems* - **J. Shinoda, O. B. Kazanci, S-I. Tanabe, B. W. Olesen** : <https://www.sciencedirect.com/science/article/pii/S0360132319303609> (12/05/2023)
- [47] *A simple method for validating a simulation model of a radiant ceiling panel with thermal energy storage* - **A. Gallardo, U. Berardi** : <https://iopscience.iop.org/article/10.1088/1742-6596/2069/1/012119> (15/05/2023)
- [48] *Generation of a simulation model for chilled PCM ceilings in TRNSYS and validation with real scale building data* - **M. Yasin, E. Scheidemantel, F. Klinker, H. Weinläder, S. Weismann** : <https://iopscience.iop.org/article/10.1088/1742-6596/2069/1/012119> (20/05/2023)

A Solar Heat Gain Schedule (SHG1)

Time	[W]
00:00	0
05:36	25
06:48	50
07:36	75
08:24	100
09:12	125
10:24	150
14:12	125
15:12	100
16:12	75
17:12	50
18:00	25
19:12	0
00:00	0

Figure 56: Heat rate and schedule of the experimental solar heat gains (SHG1).

B Lab Temperatures for All Scenarios

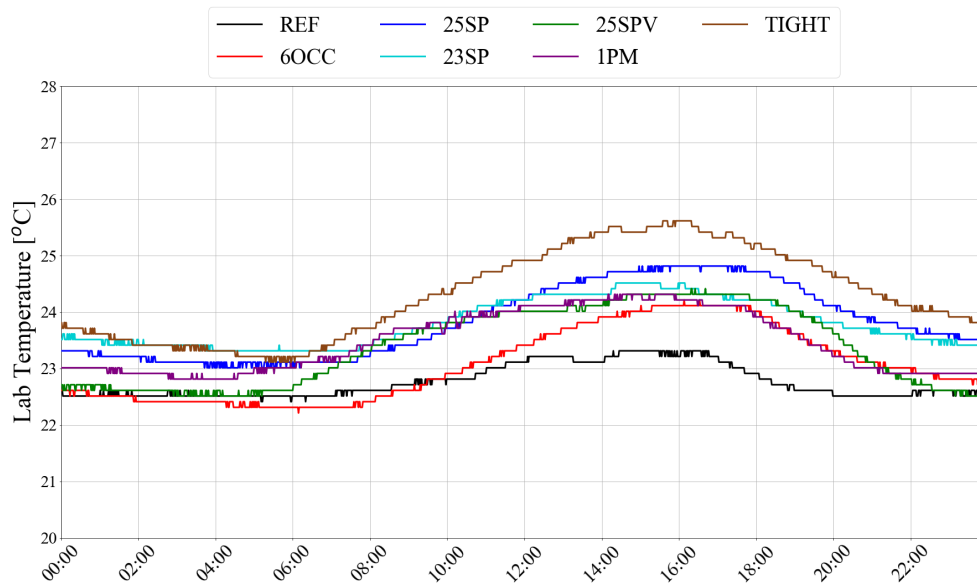


Figure 57: Lab Temperatures for All Scenarios.

C Models Technical Drawings

Dimensions in the following technical drawings are in mm.

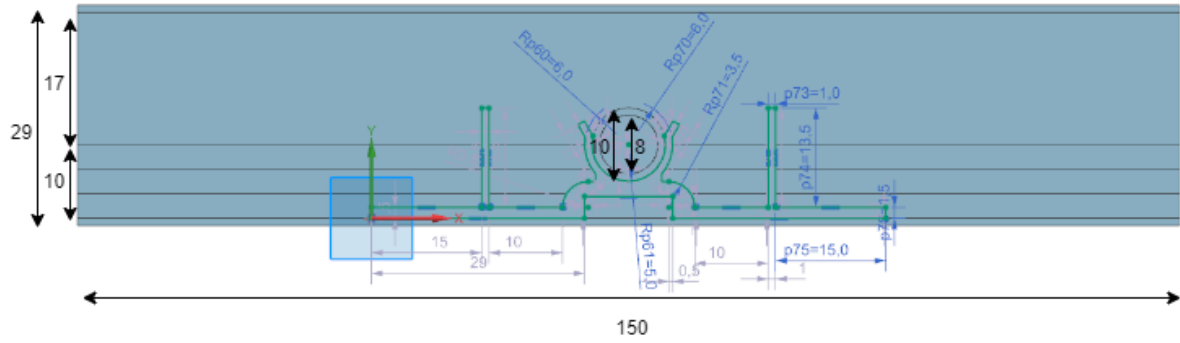


Figure 58: 2D model technical drawing.

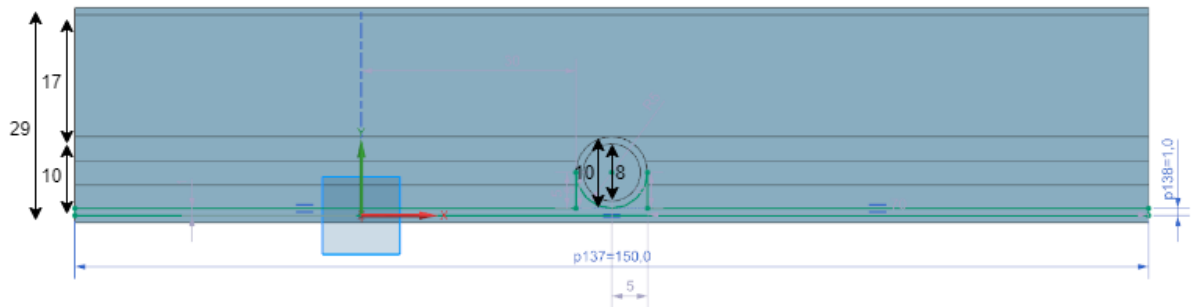


Figure 59: 2D simpler model technical drawing.

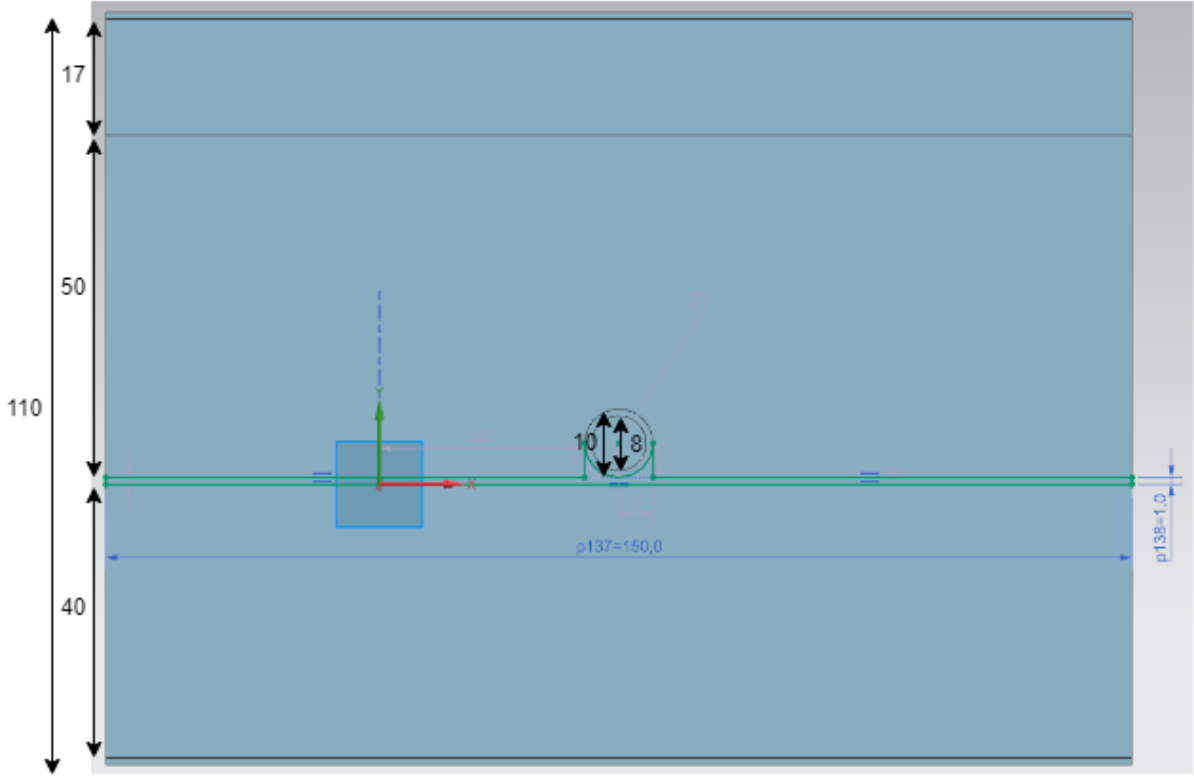


Figure 60: 2D TABS equivalent model technical drawing.